OPPORTUNITIES AND CHALLENGES OF ROBOTICALLY ASSISTED 3D PRINTING OF SHELL STRUCTURES

A Dissertation

by

MEHDI FARAHBAKHSH

Submitted to the Graduate and Professional School of
Texas A&M University
in partial fulfillment of the requirements for the degree of

DOCTOR OF PHILOSOPHY

Chair of Committee,	Stephen Mark Caffey
Co-Chair of Committee,	Zofia K. Rybkowski
Committee Members,	Negar Kalantar
	Patrick Suermann
Head of Department,	Gregory Anthony Luhan

December 2021

Major Subject: Architecture

ABSTRACT

Understanding the interdependency of design, material, fabrication process, and environmental stimuli in large-scale Additive Manufacturing (AM) processes is significant. This study aims to assess the potential and limitations associated with robotically assisted AM of scaffold-free shell structures at macro- and meso-scales. A workflow consisting of four steps (design, fabrication, digital reconstruction, and digital and physical analysis) was developed to study the impact of three process parameters (L, the distance between hypothetical nodes on the toolpath, H_2, the standoff distance of the nozzle, and T, the delay time at each point) on the interlayer bond strength of 3D printed structures with a clay-based material.

This paper proposes a technical approach by manipulating process parameters that alter the geometry of the layers on the meso-scale to emulate densification and to enhance friction between consecutive layers in robotically assisted paste AM processes. The difficulties related to simulating and predicting AM processes in a digital analysis method are described, as are results from the standard flexural test performed on 95 printed specimens. Flexural tests showed that manipulating the H_2 parameter based on the defined criteria improved interlayer bond strength under shear by 41.2% on average. Since the results are inconsistent, however, it was not possible to detect any obvious impact of the T parameter on interlayer bond strength.

Additionally, this dissertation delves into the details of a nested robotic fabrication strategy at the macro-scale and discusses the design requirements for

constructing structures taller than the robot's maximum reach. According to the specified design requirements, a case study was carried out in order to explore the possibilities and challenges associated with constructing stackable geometries using nested 3D printing. Clay was utilized for the first time in a robotic AM process to create a dissolvable formwork. This research highlights the need to integrate cutting-edge technological considerations into the design process, which can lead to design innovations and structural integrity.

DEDICATION

To my mother for all her love, to my father for all his support and dreams for me, to my sister for all her sacrifices, to my wife for her strong spirit, and to all of those who wish to alleviate human suffering.

ACKNOWLEDGEMENTS

There are so many people who helped me along this accomplishment. This work would not be possible without their support. I would like to take this opportunity to thank my committee chair, Dr. Stephen Caffey who supported me since the very morning I started my journey at Texas A&M University. A huge thank you goes to my co-chair, Dr. Zofia Rybkowski, who believed in me, helped me create and pursue my goals, and supported me every step of the way. I would also like to express my deepest gratitude to my mentor, friend, and colleague, Dr. Negar Kalantar. Thank you to Dr. Patrick Suermann who has supported me beyond my expectations.

CONTRIBUTORS AND FUNDING SOURCES

Contributors

This work was supervised by a dissertation committee consisting of Dr. Stephen Mark Caffey (Chair), Dr. Zofia Rybkowski (Co-Chair), and Dr. Negar Kalantar of the Department of Architecture and Dr. Patrick Suermann of the Department of Construction Science.

Mrs. Umme Zakira of the Department of Civil Engineering assisted with the flexural testing in Chapter 3. Mr. Ibrahim Onifade of the Department of Civil Engineering also served as a consultant for the digital analysis investigations.

The nesting design approach described in chapter 4 was developed with the assistance of Mr. Alireza Borhani of California College of the Arts and was published in 2021.

All other work conducted for the dissertation was completed by the author independently.

Funding Sources

This work was partially funded by the X-Grants Program: A President's Excellence Fund initiative at Texas A&M University.

GLOSSARY

3D Printing	"the fabrication of objects through the deposition of a material using a print head, nozzle, or another printer technology. (Term often used synonymously with additive manufacturing; in particular associated with machines that are low end in price and/or overall capability.)"[1]
3D Scanning	"a method of acquiring the shape and size of an object as a 3-dimensional representation by recording x,y,z coordinates on the object's surface and through software the collection of points is converted into digital data"[2]
Additive Manufacturing	"a process of joining materials to make objects from 3D model data, usually layer upon layer, as opposed to subtractive manufacturing methodologies."[2]
Cold Joint	"a joint or discontinuity resulting from a delay in placement of sufficient duration to preclude intermingling

[1] ASTM International. (2013). F2792-12a - Standard Terminology for Additive Manufacturing Technologies. Rapid Manufacturing Association, West Conshohocken, PA, p. 1.
[2] ASTM International. (2013). F2792-12a - Standard Terminology for Additive Manufacturing Technologies. Rapid Manufacturing Association, West Conshohocken, PA, p. 2.

	and bonding of the material, or where mortar or plaster rejoin or meet”[3]
Filament	“a slender threadlike object or fiber”[4]
Paste	“a thick, soft, moist substance typically produced by mixing dry ingredients with a liquid.”[4]

[3] ACI CT-13. (2013). ACI Concrete Terminology. American Concrete Institute, Farmington Hills, MI, p. 15.
[4] Oxford English Dictionary Online. June 2021. Oxford University Press. http://www.oed.com (accessed September 04, 2021)

TABLE OF CONTENTS

Page

LIST OF FIGURES

Page

LIST OF TABLES

1. INTRODUCTION

Additive manufacturing (AM), commonly referred to as 3D printing, is a process of constructing objects from three-dimensional (3D) model data, in which the material is horizontally extruded and deposited layer by layer (ASTM International 2013; Guo and Leu 2013). In contrast to its earliest stages of development in the late 1980s (Guo and Leu 2013), AM currently offers broad applications ranging from small-scale fabrications such as jewelry, pottery, and medical instruments to large-scale construction and applications in the heavy manufacturing industry (Buchanan and Gardner 2019; Gosselin et al. 2016; Khoshnevis 2004).

While traditional construction methods have established rules and regulations, there is a lack of standards for evaluating large-scale AM processes. Examples in the literature, however, show researchers' efforts to define a new set of regulations to bridge this gap (Zareiyan and Khoshnevis 2017a). Moreover, precise computer-controlled deposition of material has enabled AM processes to reduce resource consumption, speed up construction processes, and reduce total construction costs compared to conventional large-scale construction. However, Buswell (2007) argued that neither speed nor cost are critical reasons for the growing interest in AM for large-scale construction; its popularity is more likely due to enhanced functional performance and geometrically rich building elements.

Concrete’s mechanical properties, broad availability, low price, and adjustable setting time make it the primary candidate to be used in large-scale 3D printing projects.

The concrete industry, however, has raised some concerns about global carbon emissions (IEA 2019). Researchers have addressed the issue by utilizing cement substitutes such as fly ash, but the CO_2 emission remains substantial. One way to reduce the CO_2 impact of large-scale AM is to use *in situ* resources. The minerals found in the Earth's crust provide a naturally sourced material palette to create a clay-based material that has been utilized in architecture throughout history and may be employed in contemporary construction technologies such as large-scale additive manufacturing. Generally, with regards to a clay-based material's mechanical properties being inferior compared to concrete, both design and technical strategies are required to incorporate this kind of material in large-scale AM successfully.

Robotic fabrication technologies have facilitated the production of nonstandard architectural forms. The robot's reach and freedom of movement in the space, however, have remained challenging, affecting the size and shape of the final product.

Solutions such as cable robots (Izard et al. 2017), gantry systems (Khoshnevis 2004), telescopic booms (Keating et al. 2017), and 6-axis robotic arms equipped with one or more external axes (Zhang et al. 2018) have been developed to build large-scale structures. Nevertheless, the size of the final product is still limited to the size of the robot.

In this research, manipulation of process parameters in robotically assisted paste printing will be studied at two scales: *macro*- and *meso*-. Additionally, the effect of geometry on both structural features and new avenues of architectural design and digital

fabrication, along with the impacts of using the potentials of six-axis industrial robotic arms, will be investigated in the robotically assisted AM of shell structures.

1.1. Research Problem and Questions

Two issues have been identified on macro- and meso-scale in this research:

First, the binding between horizontal layers that can be affected by manipulating process parameters (e.g., the speed of the printhead, the rate of material deposition, the distance between the nozzle and the print surface, to name a few). While these parameters have been investigated by researchers (Bos et al. 2016; Buswell et al. 2018; Gosselin et al. 2016; Zareiyan and Khoshnevis 2017b), the role of geometry with respect to binding between layers has not yet been sufficiently treated in detail nor applied to construction projects.

Second, the vertical range that the robot may move in determines the maximum height of a 3D printed element. Several approaches to 3D printing large-scale structures have been employed in the literature. However, the size of the final product is still restricted by the reachable area of the robot.

The issue on the meso-scale has been addressed in this dissertation, and a case study was conducted for the issues on the macro-scale in order to provide the groundwork for future research. This research proposes to address the following questions:

- How and to what extent do print parameters impact the bond strength between successive layers in robotically assisted paste printing processes?

- How can an industrial robotic arm be leveraged to construct structures that exceed the vertical reach of the robot?

1.2. Background

1.2.1. The history of architectural robotics

The concept of the artificial human and the idea of self-operating machines originated in so-called primitive civilizations (de Monchaux and Goldberg 2016; Moravec 2017). There are several examples in the literature of pneumatic, hydraulic and mechanical machines resembling animals and humans, or just *automata* servants (Gera 2003; Needham 1991). The term *robot*, however, was first used in a play called "Rossum's Universal Robots", written by the Czech writer Karel Čapek in 1920. The word derives from the Czech word *robota*, meaning forced labor or serf. Isaac Asimov, later in 1942, used the word “robotics” in his short story, “Runaround,” and introduced his three laws of robotics (Barthelmess and Furbach 2014; Moravec 2017).

Contemporary architecture frames a binary concept for robots in the field: first, robot as a tool for fabrication purposes; and second, architecture as a giant robot or a machine for living in. The former implies the role of robots to free architecture from the traditional constraints of construction and their assembly by humans, while the latter challenges those approaches that consider architecture to be rigid and fixed (Lynn 2016; Mallgrave and Contandriopoulos 2006; de Monchaux and Goldberg 2016).

1.2.2. Architectural geometry

There is extensive literature on the history of architectural geometry, various technologies, and approaches (Kostof and Castillo 1995), all of which demonstrates that

enclosing a space has always been challenging. Based on available materials and technologies, some cultures benefited from corbelling, whether by using stone or adobe (Kostof and Castillo 1995; Rossi 2004). Others became proficient in building vaults and domes (Elkhateeb 2012; Huerta 2001), and for still other cultures, structures in nature along with biological systems have been rich sources of inspiration for tackling technical problems in architecture and engineering (Magna et al. 2012; Vincent 2009).

Vaults and domes evolved markedly during history and made it possible to construct masonry buildings with wider spans and higher spaces. This evolution includes geometrical innovations such as pendentives, which are structural elements that facilitate the transition from a rectangular space to a circular dome; and buttresses, which are structural elements positioned against or projecting from a wall that support a vault or dome (Elkhateeb 2012; Huerta 2001; Sectionnelle and Mosquées 2010). Indeed, equilibrium is achieved through geometry and has made it possible to construct safe masonry structures.

Inspired by nature, Vincent (2009) has pointed out the potential of biomimetics, and its excellent applications in problem-solving by recognizing patterns in nature the way problems are solved in biology and engineering. Mengez (2012) has provided the definitions of morphogenetic and evolutionary computational design and has described the differences between computer-aided and computational design in architecture. He argues that computational design is about the process of design and defining systems capable of adjusting the design process based on the feedback information, while

computer aided design is about the modeling of objects and designing static digital constructs.

1.2.3. Paste additive manufacturing

Additive manufacturing has found a wide range of applications in the jewelry, pottery, aerospace, motor vehicle, medical, and architecture industries (Bhardwaj et al. 2019; Buchanan and Gardner 2019; Gosselin et al. 2016; Khoshnevis 2004). When it comes to large-scale AM with paste materials in architecture and construction, the Contour Crafting project, concrete printing project at Loughborough University, and the D-Shape project are considered the benchmark technologies over the last decade (Gosselin et al. 2016). The Contour Crafting project, developed by researchers at the University of Southern California (Khoshnevis 2004), utilizes a cementitious material. This project is based on generating a formwork by 3D printing of two layers with 13_{mm} thickness and later, filling the formwork with concrete. The nozzle is mounted on a three-axis crane designed for onsite construction. The concrete printing project at Loughborough University (Buswell et al. 2007), like the Contour Crafting project, also uses a nozzle mounted on a three-axis crane for material deposition. The nozzle size in this project is 9_{mm} in diameter, and the layer thickness is 4-6 $_{mm}$. The D-Shape project by Enrico Dini (Cesaretti et al. 2014) uses binder jetting technology. Binder jetting is an AM process wherein a liquid bonding agent is deposited on a layer of powder (ASTM International 2013). D-Shape technology also uses a three-axis overhead crane to deposit a binding agent and selectively solidify a large-scale sand-bed. In this technique, the powder material serves as the additional support in other mentioned technologies. Once

the printing process is over, the printed piece is taken out, and the remaining powder material can be used in the process again (Cesaretti et al. 2014; Gosselin et al. 2016). To date, most research on AM with paste, concrete, cement-based materials, or clay, is based upon one of those three mentioned projects, resulting in proposed amendments to improve productivity and scale. Zhang et al. (2018) proposed to deploy a team of mobile robots, and Keating et al. (2017) presented a platform composed of a large 4-degree-of-freedom (DOF) hydraulic arm with a smaller 6-DOF electric robotic arm to expand the reach of the system along with the work area. In terms of structural features in an AM process, Zareiyan and Khoshnevis (2017) investigated the role of material in interlayer adhesion and strength in a Countour Crafting process. Gosselin et al. (2016) mentioned the geometric impact of the print strategy and the crucial role of nozzle orientation in the binding between layers. However, they did not construct any specimen or structure using the adjustment of the nozzle orientation.

1.2.4. Robotic 3D printing

Wu et al. (2016) challenged the productivity of the construction industry in the US and appreciated AM technology as an innovative construction technique. Nevertheless, the authors presented a critical review of AM processes and suggested more research to consolidate the stability and expand the application of AM in the construction industry.

There are many precedents for large-scale AM with paste. In terms of machinery, there are four distinct categories in the literature. The first group uses a gantry system, an overhead three-axis machine where the printhead is mounted on the bridge-like structure

(Khoshnevis 2004; Labonnote et al. 2016). Although this system provides decent access to the work area, it must span the entire print area.

The second group comprises a mounted printhead on a telescopic-foldable boom that was adapted from the existing concrete pump machines (“COBOD” n.d.; Mechtcherine et al. 2019). The goal of the research, as the authors stated, was to develop a technology for large-scale on-site 3D printing with existing concrete standards. The stability and accuracy of this system in farther points relative to the base structure are still under debate.

The third group engages a three-axis cable-suspended machine, which is a "type of parallel manipulator in which flexible cables are used as actuators” (“Hybrid INDustrial CONstruction” n.d.). This system is a three-axis machine that is relatively dynamic and straightforward, and the fact that the structural frame should be noticeably larger than printed objects makes the use of this system heavily dependent on the available space around the work area. Additionally, the suspension cables create significant constraints in the job site.

The fourth group of projects includes six-axis robot arms for 3D printing paste. Due to abundant supply, along with relatively low prices, high precision, and easy-to-control features (Mechtcherine et al. 2019), the fields of architecture and construction have shown great interest in industrial robot arms in the last decade (“CyBe Construction” n.d.; “XtreeE” n.d.; Lindemann 2018; Zhang et al. 2018). Although limited working space has been introduced as a disadvantage of using robot arms, Zhang

et al. (2018) and Keating et al. (2017) have devised solutions to expand the work area of this group of projects.

In all the projects mentioned above, the orientation of the nozzle is perpendicular to the print bed. However, using a six-axis robot can offer the opportunity to adjust the orientation of the printhead while printing complex geometries. This adjustment could minimize or free the large-scale AM processes from making additional support, which is both costly and time-consuming, and therefore, optimize resource consumption.

1.3. Research Objectives and Significance

From the preceding discussion, the following research objectives were defined:

A productive material deposition approach, along with smart material selection and architectural geometry, should be deployed to create nonvertical surfaces when using the AM process. In order to address architectural and structural issues, geometrical manipulations in robotically assisted paste printing were tackled in two different scales, *macro-* and *meso-*. It was expected that in meso-scale, manipulation of the process parameters would impact the structural features of the final product in paste 3D printing, in particular the binding between layers. It was also expected that, at the macro-scale, devising solutions for the print strategy, e.g., adjusting the nozzle orientation based on the curvature of the print surface, and designing compound geometries, would expand the domain of possibilities and to some extent, would decrease the scale limitations of an AM process with paste materials.

It seemed essential to establish a feedback loop linking geometry, material, simulation, and manufacturing in order to make large scale AM structures. A design

approach that incorporates technical considerations in a robotically assisted AM process can be advantageous to circumvent the size restriction of 3D printed elements.

The mentioned research objectives were addressed through design strategy, technical strategy, or both as presented in Table 1.1.

Table 1.1: Research objectives and solution categories

Research objectives	Design strategy	Technical strategy
Improve interlayer bond strength	--	Manipulating process parameters
Building structures taller than the robot's reachable area	Nesting	--
Scaffold free AM of nonvertical surfaces	Compound geometries	Adjusting the orientation of the nozzle

1.4. Research Methodology

The term *reflection-in-action* was coined by Donald Schon to highlight design activity to solve problems arising out of practical life contexts (Groat, L. and Wang, D., 2013). As Linda Groat (2013) clarifies, in research, action research that is derived from Schon's concept is the logic of how factors within the situation relate to each other as the process moves toward an experimental goal. Design-decision research, as she states, is a more focused version of action research. Unlike in action research, in which the researcher is still outside of the situation, however, in design-decision research a researcher can be a player in the process. In this sense, a researcher not only makes decisions but also assesses those decisions from the perspective of research (Groat and Wang 2013).

It may be helpful for future scholars to know the route that was followed in this dissertation. The author started working with an ABB robotic arm for the first time in

August 2018. Due to the absence of a robot technician at the lab and a lack of online resources on how to operate a robotic arm, the author had to self-teach how to jog the robot (move the robot joints) using a device called flex pendant. It took him a few days locate the enabling button on the back of the flex pendant that activates the robot's motors. It is a safety feature embedded in the robot controller that ensures the operator is present and watching the robot's movements.

ROS (Robot Operating System), the most widely used robot controller platform, is a versatile platform for developing robot software. It is a set of tools, libraries, and conventions designed to make it easier to create sophisticated and resilient robot behavior across a broad range of robotic systems (“ROS” 2007). Similar to dealing with low-level programing languages, however, programming with ROS is neither simple nor desirable for architects. At the time, two plugins (Taco and HAL) for Rhino 5 (a 3D modeling software) and Grasshopper (a visual programming environment that runs on Rhino) were available that allowed users to operate an ABB robotic arm. The author began using Taco and subsequently moved to the HAL plugin due to Taco's restrictions. Later in December 2018, the author was invited to join a multi-disciplinary research group researching in situ resource utilization for additive manufacturing in construction. As an architect, the author was expected to develop design and technical solutions to 3D print architectural forms using a novel material provided by the research group. A medium-scale 3D printer (Delta WASP 4070) was operational at the Advanced Infrastructure Materials and Manufacturing (AIMM) lab at the Center for Infrastructure Renewal (CIR). The nozzle size, however, was insufficient for the project and the

material delivery system was incapable of delivering enough material to the 3D printer. Therefore, the author decided to attach an extruder to the ABB robotic arm and build a material delivery system based on the rheological requirements of the provided material. Robotically assisted AM is a relatively new technology, and we were unable to purchase a reliable product on the market that can be used for the project. Instead, the author designed, built & developed all of the required tools on my own (Figure 1.1).

Figure 1.1: Several extruders were designed and tested

All the tools used in this research, including end effectors and microcontrollers, were designed, fabricated, and programmed by myself (Figure 1.2). Eight months were spent to build and test several iterations to optimize the extruder and material delivery system. While it was only possible to extrude the material in the first iteration, the fifth iteration provided an adequate level of control over the material deposition process

(Figure 1.3). The first iteration of the material delivery system relied entirely on pneumatic pressure without the use a diaphragm (Figure 1.3a), with the material tank mounted on the robotic arm. This method not only resulted in inconsistent material flow, but also restricted the size of the material tank owing to the robotic arm's load capacity restriction.

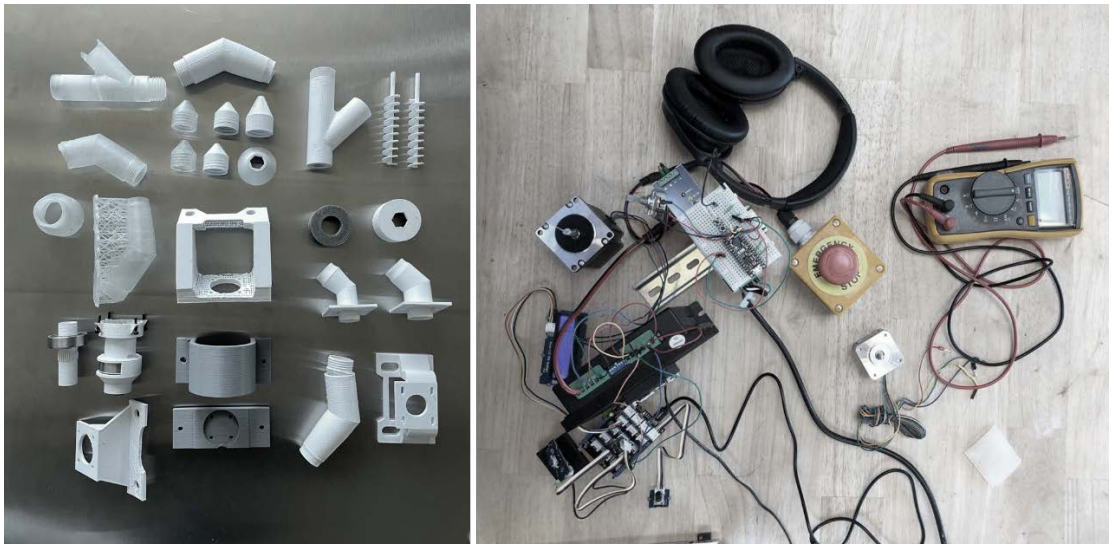

Figure 1.2: The left figure provides some of the failed examples of the extruder design, 3D printed with Acrylonitrile Styrene Acrylate (ASA), a thermoplastic filament. The right figure shows an effort for programming a microcontroller (Arduino Uno) that controlled the stepper motor in the extruder

The second iteration of the material delivery system was an upgrade to the first (Figure 1.3b). To improve the consistency of the material flow, a diaphragm was added to the material tank. The size of the material container was still restricted by the load capacity of the robotic arm. In both first and second versions the nozzle was located far from the mounting point. Consequently, each robot movement caused vibration in the end effector, reducing the precision of the deposition process.

The third iteration of the material delivery system consisted of a material tank and a diaphragm inside it that was pressurized with a pneumatic system and connected to the robot's end effector through a hose (Figure 1.3c and Figure 1.3d). a bespoke extruder was developed for the third iteration that featured a stepper motor that applied mechanical pressure to ensure consistent and precise material flow. The fourth iteration used the same material container in the third iteration, while the extruder was modified to achieve a unified 3D printed body (Figure 1.3e and Figure 1.3f).

The optimized material delivery system and the extruder attached to the robotic arm enabled me to 3D print several materials supplied by our research group. While three-axis 3D printers have a restricted range of motion and the direction of the extruder is fixed and always perpendicular to the print bed, using a six-axis robotic arm offered greater flexibility and opportunities to explore design concepts and fabrication techniques. Most AM processes use G-code (the most used programming language for computer numerical control systems). A unique technique was devised for robot tool pathing in Grasshopper and HAL; as a result, technical considerations for robot programming and material delivery systems could be included in the architectural design process.

Figure 1.3: Several iterations were developed and tested in order to create an optimal extruder for depositing the novel material supplied by the research group

After almost one year of experimenting with the design process and technical considerations, two research gaps were identified in the literature. The dissertation committee suggested that the focus should be on one issue that was more relevant to the research group's work and discuss another research question (a topic that the author had

been exploring with the students in the architectural and construction robotics class) as a case study.

Outlining the research process workflow in collaboration with the engineering department at Texas A&M University helped determine the indispensable skillset and tools for project completion. Developing steps one and two of the process required design, programming, and fabrication skills, while step three called for access to an X-ray machine capable of scanning medium-sized samples.

There was an X-ray machine at the CIR at Texas A&M University, but only samples with a maximum size of five inches could be scanned with that machine, while specimens of eleven inches in length were required to be scanned. Additional X-ray equipment was located on campus in the Petroleum Department. It was a piece of customized medical X-ray equipment that was used to scan dense objects composed of concrete and asphalt.

The outcome of the scanning step was a series of 2D images that could be used in image processing procedure. Several experiments were conducted with ImageJ[5], SimpleWare[6], and Mimics[7], to name a few, which are often used in the medical, dentistry, and additive manufacturing industries. Mimics was the best match for the

[5] an image processing software written in Java that was created at the National Institutes of Health and the Laboratory for Optical and Computational Instrumentation (Schneider et al. 2012)
[6] a 3D image processing program created by Synopsys Inc.
[7] a 3D image processing program developed by Materialise NV

current research requirements since it was simple to use, and the generated 3D model was optimized to be utilized in COMSOL[8].

The research questions mentioned above were tackled in this dissertation by developing a workflow at the meso-scale and then conducting case studies at a macro-scale. The second chapter is an expanded version of a previously published article that elaborates on the suggested methodology for examining the effect of process parameters on layer binding in an additive manufacturing process using paste. Additionally, the chapter discusses physical and digital analysis techniques. The third chapter is a forthcoming article that examines the effect of three chosen process parameters on the interlayer bond strength at the meso-scale using paste AM, and contains detailed findings and analysis. A nested robotic fabrication strategy, also previously published as another article, is introduced in chapter four of this dissertation, which in a case study explores the possibility of building a stackable object taller than the robot's reachable zone.

[8] a finite element analysis software

1.5. References

Anton, A., Yoo, A., Bedarf, P., Reiter, L., Wangler, T., and Dillenburger, B. (2019). "Vertical Modulations Computational design for concrete 3D printed columns." *Ubiquity and Autonomy - Paper Proceedings of the 39th Annual Conference of the Association for Computer Aided Design in Architecture, ACADIA 2019*, (October), 596–605.

ASTM International. (2013). *F2792-12a - Standard Terminology for Additive Manufacturing Technologies*. *Rapid Manufacturing Association*, West Conshohocken, PA.

Bajpayee, A., Farahbakhsh, M., Zakira, U., Pandey, A., Ennab, L. A., Rybkowski, Z., Dixit, M. K., Schwab, P. A., Kalantar, N., Birgisson, B., and Banerjee, S. (2020). "In situ Resource Utilization and Reconfiguration of Soils Into Construction Materials for the Additive Manufacturing of Buildings." *Frontiers in Materials*, 7(March), 1–12.

Bard, J., Mankouche, S., and Schulte, M. (2012). "Morphfaux: Probing the proto-synthetic nature of plaster through robotic tooling." *ACADIA 2012 - Synthetic Digital Ecologies: Proceedings of the 32nd Annual Conference of the Association for Computer Aided Design in Architecture*, 2012-Octob(1), 177–186.

Barthelmess, U., and Furbach, U. (2014). "Do we need Asimov's Laws?" *arXiv, Cornell University*, <http://arxiv.org/abs/1405.0961> (Mar. 17, 2020).

Bhardwaj, A., Jones, S. Z., Kalantar, N., Pei, Z., Vickers, J., Wangler, T., Zavattieri, P., and Zou, N. (2019). "Additive Manufacturing Processes for Infrastructure Construction: A Review." *Journal of Manufacturing Science and Engineering*,

141(9).

Buchanan, C., and Gardner, L. (2019). “Metal 3D printing in construction: A review of methods, research, applications, opportunities and challenges.” *Engineering Structures*, Elsevier, 180, 332–348.

Burger, J., Lloret-Fritschi, E., Scotto, F., Demoulin, T., and Gebhard, L. (2009). “Research Collection.” *3D PRINTING AND ADDITIVE MANUFACTURING*, 7(2).

Burger, J., Lloret-Fritschi, E., Scotto, F., Demoulin, T., Gebhard, L., Mata-Falcón, J., Gramazio, F., Kohler, M., and Flatt, R. J. (2020). “Eggshell: Ultra-thin three-dimensional printed formwork for concrete structures.” *3D Printing and Additive Manufacturing*, 7(2), 49–59.

Buswell, R. A., Silva, W. R. L. De, Jones, S. Z., Dirrenberger, J., Leal de Silva, W. R., Jones, S. Z., and Dirrenberger, J. (2018). “3D printing using concrete extrusion: A roadmap for research.” *Cement and Concrete Research*, Elsevier, 112(October 2017), 37–49.

Buswell, R. A., Soar, R. C., Gibb, A. G. F., and Thorpe, A. (2007). “Freeform Construction: Mega-scale Rapid Manufacturing for construction.” *Automation in Construction*, 16(2), 224–231.

Cesaretti, G., Dini, E., De Kestelier, X., Colla, V., and Pambaguian, L. (2014). “Building components for an outpost on the Lunar soil by means of a novel 3D printing technology.” *Acta Astronautica*, Elsevier, 93, 430–450.

Craveiro, F., Duarte, J. P., Bartolo, H., and Bartolo, P. J. (2019). “Additive manufacturing as an enabling technology for digital construction: A perspective on Construction 4.0.” *Automation in Construction*, Elsevier, 103(October 2018), 251–

267.

“CyBe Construction.” (n.d.). .

Doyle, S. E., and Hunt, E. L. (2019). “Dissolvable 3D Printed Formwork.” *ACADIA*, 178–187.

Elkhateeb, A. A. (2012). “Domes in the Islamic Architecture of Cairo City: A Mathematical Approach.” *Architecture, Systems Research and Computational Sciences. Nexus Network Journal*, K. Williams and R. Fletcher, eds., Birkhäuser, Basel.

Farahbakhsh, M., Kalantar, N., and Rybkowski, Z. (2020). “Impact of robotic 3D printing process parameters on bond strength.” *40th Annual Conference of the Association for Computer Aided Design in Architecture, ACADIA 2020*.

Feng, P., Meng, X., Chen, J. F., and Ye, L. (2015). “Mechanical properties of structures 3D printed with cementitious powders.” *Construction and Building Materials*, Elsevier Ltd, 93, 486–497.

Gera, D. L. (2003). *Ancient Greek ideas on speech, language, and civilization*. Oxford University Press, New York.

Gosselin, C., Duballet, R., Roux, P., Gaudillière, N., Dirrenberger, J., and Morel, P. (2016). “Large-scale 3D printing of ultra-high performance concrete - a new processing route for architects and builders.” *Materials and Design*, Elsevier Ltd, 100, 102–109.

Groat, L. N., and Wang, D. (2013). *ArchitecturAl reseArch Methods*. John Wiley & Sons, Inc, Hoboken, New Jersey.

Guo, N., and Leu, M. C. (2013). “Additive manufacturing: Technology, applications and research needs.” *Frontiers of Mechanical Engineering*, 8(3), 215–243.

Hosseini, E., Zakertabrizi, M., Korayem, A. H., and Xu, G. (2019). “A novel method to enhance the interlayer bonding of 3D printing concrete: An experimental and computational investigation.” *Cement and Concrete Composites*, 99(March), 112–119.

Huerta, S. (2001). “Mechanics of masonry vaults: The equilibrium approach.” *Historical Constructions*, P. B. Lourenço and P. Roca, eds., Guimarães, 47–70.

“Hybrid INDustrial CONstruction.” (n.d.). .

“ICON.” (2021). <https://www.iconbuild.com/vulcan> (Feb. 6, 2021).

IEA. (2019). “World Energy Outlook 2019.” *World Energy Outlook 2019*, 1.

Izard, J., Dubor, A., Hervé, P., and Cabay, E. (2017). “Large Scale 3D Printing with Cable-Driven Parallel Robots.” *Construction Robotics*.

Keating, S. J., Leland, J. C., Cai, L., and Oxman, N. (2017). “Toward site-specific and self-sufficient robotic fabrication on architectural scales.” *Science Robotics*, 2(5).

Keita, E., Bessaies-Bey, H., Zuo, W., Belin, P., and Roussel, N. (2019). “Weak bond strength between successive layers in extrusion-based additive manufacturing: measurement and physical origin.” *Cement and Concrete Research*, Elsevier, 123(November 2018), 105787.

Khan, M. S., Sanchez, F., and Zhou, H. (2020). “3-D printing of concrete: Beyond horizons.” *Cement and Concrete Research*, 133(December 2019).

Khoshnevis, B. (2004). “Automated construction by contour crafting, related robotics and information technologies.” *Automation in Construction*, 13, 5–19.

Kloft, H., Krauss, H. W., Hack, N., Herrmann, E., Neudecker, S., Varady, P. A., and Lowke, D. (2020). “Influence of process parameters on the interlayer bond strength of concrete elements additive manufactured by Shotcrete 3D Printing (SC3DP).” *Cement and Concrete Research*, 134(December 2019).

Kostof, S., and Castillo, G. (1995). *A history of architecture*. Oxford University press, New York.

Labonnote, N., Rønnquist, A., Manum, B., and Rüther, P. (2016). “Additive construction: State-of-the-art, challenges and opportunities.” *Automation in Construction*, Elsevier B.V., 72, 347–366.

Le, T. T., Austin, S. A., Lim, S., Buswell, R. A., Law, R., Gibb, A. G. F., and Thorpe, T. (2012). “Hardened properties of high-performance printing concrete.” *Cement and Concrete Research*, 42(3), 558–566.

Lindemann, H. (2018). “3D printing with concrete: ‘Pushing the boundaries of kinematics’, Robot-controlled production in a unique system.”

Lu, B., Li, M., Wong, T. N., and Qian, S. (2021). “Effect of printing parameters on material distribution in spray-based 3D concrete printing (S-3DCP).” *Automation in Construction*, 124(February).

Lynn, G. (2016). “Giant Robots.” *Log*, 36, 12–16.

Magna, R. La, WAIMER, F., and Knippers, J. (2012). “Nature-inspired generation scheme for shell structures.” *The International Symposium of the IASS-APCS*,

Seoul, South Korea.

Mallgrave, H. F., and Contandriopoulos, C. (Eds.). (2006). *Architectural theory, Volume II, An anthology from 1871-2005*. Blackwell Publishing, Malden, MA.

Mansoori, M., and Palmer, W. (2018). “Handmade by Machine : A Study on Layered Paste Deposition Methods in 3D Printing Geometric Sculptures.” (June).

Marchment, T., and Sanjayan, J. (2019). *Method of enhancing interlayer bond strength in 3D concrete printing*. *RILEM Bookseries*, Springer International Publishing.

Marchment, T., Xia, M., Dodd, E., Sanjayan, J., and Nematollahi, B. (2017). “Effect of delay time on the mechanical properties of extrusion-based 3D printed concrete.” *ISARC 2017 - Proceedings of the 34th International Symposium on Automation and Robotics in Construction*, (Isarc), 240–245.

Mechtcherine, V., Nerella, V. N., Will, F., Näther, M., Otto, J., and Krause, M. (2019). “Large-scale digital concrete construction – CONPrint3D concept for on-site, monolithic 3D printing.” *Automation in Construction*, Elsevier, 107.

de Monchaux, N., and Goldberg, K. (2016). “Death and Robots.” *Log*, (36), 17–26.

Moravec, H. P. (2017). “Robot.” *Encyclopædia Britannica, inc.*, <https://www.britannica.com/technology/robot-technology> (Mar. 17, 2020).

Naboni, R., and Breseghello, L. (2018). “Fused Deposition Modelling Formworks for Complex Concrete Constructions.” *SIGraDi 2018*, 700–707.

Nee, A. Y. C., Seow, K. W., and Long, S. L. (1986). “Designing Algorithm for Nesting Irregular Shapes With and Without Boundary Constraints.” *Annals of the ClRP*, 107–110.

Needham, J. (1991). *Science and Civilisation in China, Volume 2, History of Scientific Thought*. Cambridge, New York.

Nerella, V. N., Hempel, S., and Mechtcherine, V. (2019). “Effects of layer-interface properties on mechanical performance of concrete elements produced by extrusion-based 3D printing.” *Construction and Building Materials*, 205, 586–601.

Nerella, V. N., and Mechtcherine, V. (2017). “MICRO-AND MACROSCOPIC INVESTIGATIONS ON THE INTERFACE BETWEEN LAYERS OF 3D PRINTED CEMENTITIOUS ELEMENTS Textile Reinforced Concrete View project SHCC Creep and Durability View project.” (September).

Panda, B., Mohamed, N. A. N., Paul, S. C., Singh, G. V. P. B., Tan, M. J., and Šavija, B. (2019). “The effect of material fresh properties and process parameters on buildability and interlayer adhesion of 3D printed concrete.” *Materials*, 12(13).

Panda, B., Paul, S. C., Mohamed, N. A. N., Tay, Y. W. D., and Tan, M. J. (2018). “Measurement of tensile bond strength of 3D printed geopolymer mortar.” *Measurement: Journal of the International Measurement Confederation*, 113(April 2017), 108–116.

Paolini, A., Kollmannsberger, S., and Rank, E. (2019). “Additive manufacturing in construction: A review on processes, applications, and digital planning methods.” *Additive Manufacturing*, Elsevier, 30(July), 100894.

Rael, R., and San Fratello, V. (2021). “Casa Covida.” <https://www.rael-sanfratello.com/made/casa-covida> (Feb. 6, 2021).

“ROS.” (2007). <www.ros.org> (Feb. 9, 2021).

Rossi, C. (2004). *Architecture and Mathematics in Ancient Egypt*. Cambridge University Press, New York.

Sanjayan, J. G., Nematollahi, B., Xia, M., and Marchment, T. (2018). "Effect of surface moisture on inter-layer strength of 3D printed concrete." *Construction and Building Materials*, Elsevier Ltd, 172, 468–475.

Santos, D. S., Santos, P. M. D., and Dias-Da-Costa, D. (2012). "Effect of surface preparation and bonding agent on the concrete-to-concrete interface strength." *Construction and Building Materials*, Elsevier Ltd, 37, 102–110.

De Schutter, G., and Lesage, K. (2018). "Active control of properties of concrete: a (p)review." *Materials and Structures/Materiaux et Constructions*, Springer Netherlands, 51(5), 1–16.

Schutter, G. De, Lesage, K., Mechtcherine, V., Nerella, V. N., Habert, G., and Agusti-Juan, I. (2018). "Vision of 3D printing with concrete — Technical, economic and environmental potentials." *Cement and Concrete Research*, Elsevier, 112(August), 25–36.

Schneider, C., Rasband, W. & Eliceiri, K. NIH Image to ImageJ: 25 years of image analysis. Nat Methods 9, 671–675 (2012). https://doi.org/10.1038/nmeth.2089

Sectionnelle, A., and Mosquées, D. E. S. (2010). "Sectional Analysis of Pendentive Dome Mosques During Ottoman Era." 6(5), 124–136.

Uliasz-Bocheńczyk, A., and Mokrzycki, E. (2020). "The potential of FBC fly ashes to reduce CO2 emissions." *Scientific Reports*, 1–9.

Vincent, J. (2009). "Biomimetic Patterns in Architectural Design." *Architectural design*,

79(6), 74–81.

Wangler, T., Lloret, E., Reiter, L., Hack, N., Gramazio, F., Kohler, M., Bernhard, M., Dillenburger, B., Buchli, J., Roussel, N., and Flatt, R. (2016). “Digital Concrete: Opportunities and Challenges.” *RILEM Technical Letters*, 1, 67.

Wangler, T., Roussel, N., Bos, F. P., Salet, T. A. M., and Flatt, R. J. (2019). “Digital Concrete: A Review.” *Cement and Concrete Research*, 123(June).

Wolfs, R. J. M., Bos, F. P., and Salet, T. A. M. (2019). “Hardened properties of 3D printed concrete: The influence of process parameters on interlayer adhesion.” *Cement and Concrete Research*, Elsevier, 119(January), 132–140.

“XtreeE.” (n.d.). .

Zareiyan, B., and Khoshnevis, B. (2017a). “Interlayer adhesion and strength of structures in Contour Crafting - Effects of aggregate size, extrusion rate, and layer thickness.” *Automation in Construction*, Elsevier, Vienna, 81, 112–121.

Zareiyan, B., and Khoshnevis, B. (2017b). “Interlayer adhesion and strength of structures in Contour Crafting - Effects of aggregate size, extrusion rate, and layer thickness.” *Automation in Construction*, 81(June), 112–121.

Zhang, X., Li, M., Lim, J. H., Weng, Y., Tay, Y. W. D., Pham, H., and Pham, Q. C. (2018). “Large-scale 3D printing by a team of mobile robots.” *Automation in Construction*, Elsevier, 95(August), 98–106.

2. IMPACT OF ROBOTIC 3D PRINTING PROCESS PARAMETERS ON BOND STRENGTH: A SYSTEMATIC ANALYSIS USING CLAY-BASED MATERIALS

2.1. Overview

Additive manufacturing (AM), also known as 3D printing, offers advantages over traditional construction technologies, increasing material efficiency, fabrication precision, and speed. However, many AM projects in academia and industrial institutions do not comply with building codes. Consequently, they are not considered safe structures for public utilization and have languished as exhibition prototypes.

While three discrete scales—micro, meso, and macro—are investigated for AM with paste in this paper, structural integrity has been tackled on the meso scale to investigate the impact of process parameters on the bond strength between layers in an AM process. Real-world material deposition in a robotic-assisted AM process is subject to environmental factors such as temperature, humidity, the load of upper layers, the pressure of the nozzle on printed layers, etc. These factors add a secondary geometric characteristic to the printed objects that was missing in the initial digital model.

This paper introduces a heuristic workflow for investigating the impacts of three selective process parameters on the bond strength between layers of paste in the robotic-assisted AM of large-scale structures. The workflow includes a method for adding a secondary geometrical characteristic to the initial 3D model by employing X-ray computerized tomography (CT) scanning, digital image processing, and 3D reconstruction. Ultimately, the proposed workflow offers a pattern library that can be

used by an architect, and potentially artificial intelligence (AI) algorithms in automated AM processes to create robust architectural forms.

2.2. Introduction

There is no doubt that the future of architectural fabrication has strong ties to climate-change concerns and breakthrough technologies and materials for sustainable construction. Thirty-nine percent of global energy-related emissions come from the building industry, and concrete industries are responsible for 8% of all CO_2 emissions (IEA 2019). Therefore, a reliable substitution is urgently needed to address these concerns, and the challenges and opportunities of using local materials have become a hot topic again (Bajpayee et al. 2020).

Additive manufacturing (AM), commonly referred to as 3D printing, is the process of constructing objects from three-dimensional model data, in which the material is horizontally extruded and deposited layer by layer (ASTM International 2013; Guo and Leu 2013). The precise, computer-controlled deposition of material has enabled AM processes to reduce resource consumption, speed up construction processes, and reduce total construction costs compared to conventional large-scale construction. Buswell et al. (2007), however, argued that neither speed nor cost are critical reasons for the growing interest in AM for large-scale construction; its popularity is more likely due to enhanced functional performance and geometrically rich building elements.

This paper is part of a more extensive study on robotic- assisted AM of scaffold-free shell structures using a clay-based material. The main research introduces three

scales—micro, meso, and macro—that are responsible for material properties, binding between layers, and the geometry of architectural forms, respectively (Bajpayee et al. 2020) (Figure 2.1). This paper focuses on the meso scale (Figure 2.2) and introduces a novel workflow to investigate impacts of process parameters on the bond strength between layers of paste in robotic-assisted AM processes, evaluates the results, and creates a reliable benchmark for future research.

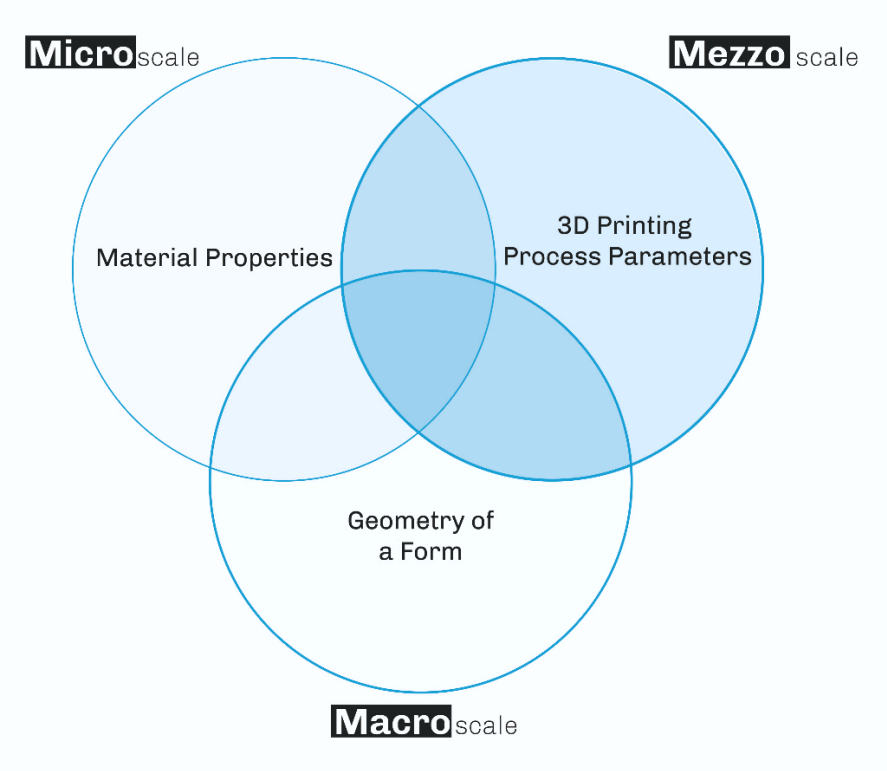

Figure 2.1: Three major areas for investigating AM with paste: material properties on micro scale; process parameters on meso scale; and the geometry of a form on the macro scale

The workflow elaborates a process to discover a pattern derived from the manipulations of three selected process parameters and investigate their impacts on the

bond strength between layers of paste in AM. Finding such a pattern will facilitate the prediction of the properties of objects printed in similar conditions.

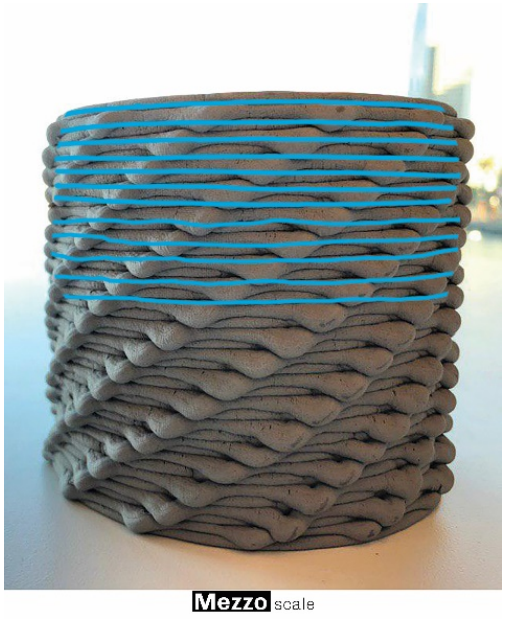

Figure 2.2: The interface between layers is categorized on the meso scale in this research

2.3. Background

During the last decade, AM has greatly improved and found several applications in the jewelry, pottery, aerospace, motor vehicle, medical, and architecture industries, to name a few (Bhardwaj et al. 2019; Buchanan and Gardner 2019; Gosselin et al. 2016; Khoshnevis 2004). The use of AM in architecture and construction can be summarized in the following three project categories (Gosselin et al. 2016):

1. The Contour Crafting project, developed by researchers at the University of Southern California (Khoshnevis 2004), utilizes a cementitious material. This project is

based on generating a formwork by 3D printing of two layers and then filling the formwork with concrete.

2. The concrete printing project at Loughborough University (Buswell et al. 2007), like the Contour Crafting project, also uses a nozzle mounted on a three-axis crane for material deposition.

3. The D-Shape project by Enrico Dini (Cesaretti et al. 2014) uses binder jetting technology. Binder jetting is an AM process wherein a liquid bonding agent is deposited on a layer of powder (ASTM International 2013).

D-Shape technology also uses a three-axis overhead crane to deposit the binding agent and selectively solidify a largescale sand bed. In this technique, the powder material serves as additional support to other mentioned technologies. Once the printing process is over, the printed piece is taken out, and the remaining powder material can be used in the process again (Cesaretti et al. 2014; Gosselin et al. 2016). In terms of structural features in an AM process, Zareiyan and Khoshnevis (2017) investigated the role of material in interlayer adhesion and strength in the Contour Crafting process. Gosselin et al. (2016) mentioned the geometric impact of the print strategy and the crucial role of nozzle orientation in the binding between layers.

The binding between horizontal layers has a significant impact on the structural integrity of printed objects. The bond strength between layers can be adjusted by manipulating process parameters (e.g., the speed of the printhead, the rate of material deposition, the distance between the nozzle and the print surface, to name a few). While

some of these parameters have been investigated by researchers (Bos et al. 2016; Buswell et al. 2018; Gosselin et al. 2016; Zareiyan and Khoshnevis 2017), the geometry of layers with respect to the binding between them has not yet been sufficiently treated in detail, nor applied to construction projects.

2.4. Workflow steps

The proposed workflow is an experimental approach that hypothesizes that the manipulations of process parameters impact the bond strength between layers in AM. Three independent process parameters that have not been extensively studied in the literature were systematically manipulated in this paper. The bond strength between layers served as the dependent variable and was measured through the novel digital analysis workflow. The workflow includes four distinct steps: design, fabrication, digital reconstruction, and analysis (Figure 2.3).

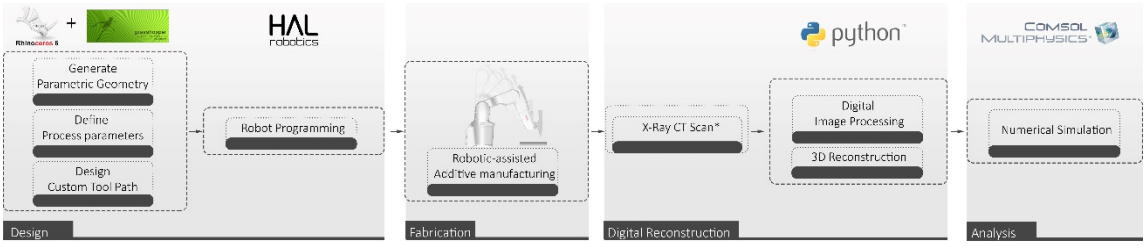

Figure 2.3: The proposed workflow includes four distinct steps: design, fabrication, digital reconstruction, and analysis

2.4.1. Design

Eight process parameters in a robotic-assisted AM process were recognized and are elaborated upon in a chart (Figure 2.4). Manipulations of the process parameters have geometric impacts on printed objects. Indeed, designing an architectural form to be

built with paste in an AM process provides the opportunity to include the process parameters in the design phase. These process parameters consist of parameters related to the programming of the robot, for instance, custom tool pathing and the speed of the robot, as well as material deposition considerations such as the extrusion flow rate and the distance between the nozzle and the print surface, to name a few. Among these eight process parameters, five have been comprehensively investigated in prior studies (Bos et al. 2016; Buswell et al. 2018; Wangler et al. 2016) and remained constant values in the current work (Figure 2.5). The following three selected process parameters, however, required additional study and have been systematically varied in this research to examine their impact on printed prototypes:

- Dn: Distance between each node
- H_2: Vertical distance between the nozzle and print surface
- T: Delay time at each node

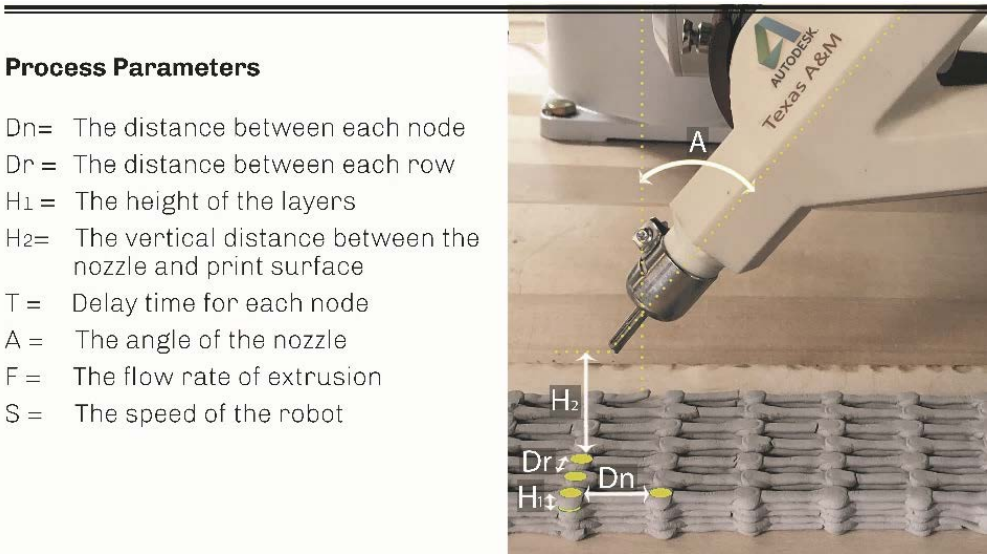

Figure 2.4: Eight process parameters

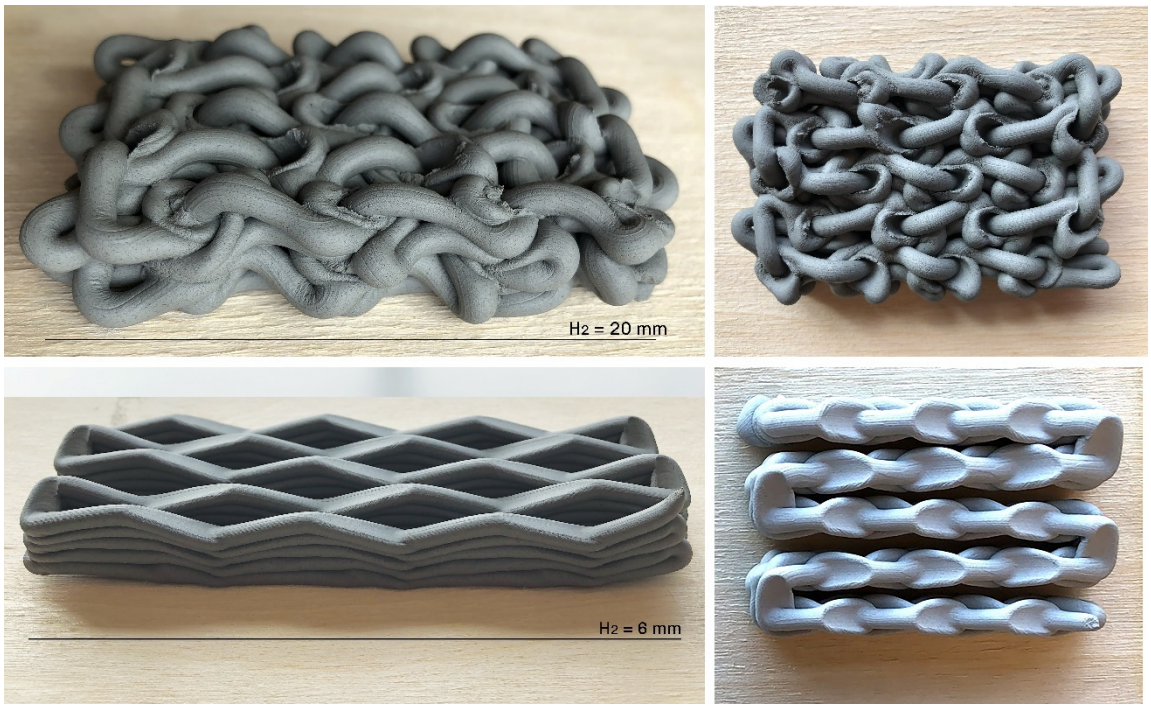

Figure 2.5: Manipulation of only one process parameter, while the other parameters remain constant, is shown in these images. The H_2 parameter (the vertical distance between the nozzle and print surface) is the only parameter that differed between the top (H_2=20 mm) and top (H_2=6 mm) 3D prints

2.4.2. Fabrication

The material deposition process in a real-world environment is subject to environmental factors. These factors add a secondary geometrical characteristic to the specimens that is missing in the initial digital model. The second step in the workflow was to physically build the digital models designed and programmed in the first step.

While most of the AM projects with concrete use progressive cavity pumps for their material delivery system, the clay-based material used in this research was not a self-flowing material. Therefore, a custom material delivery system consisting of both pneumatic and mechanical pressures was employed to create a linear pressure and to

guarantee a consistent flow of material at the extruder head. An ABB robotic arm was programmed for this step, and the selected process parameters were systematically manipulated to study challenges and potentials of each pattern (Figure 2.6).

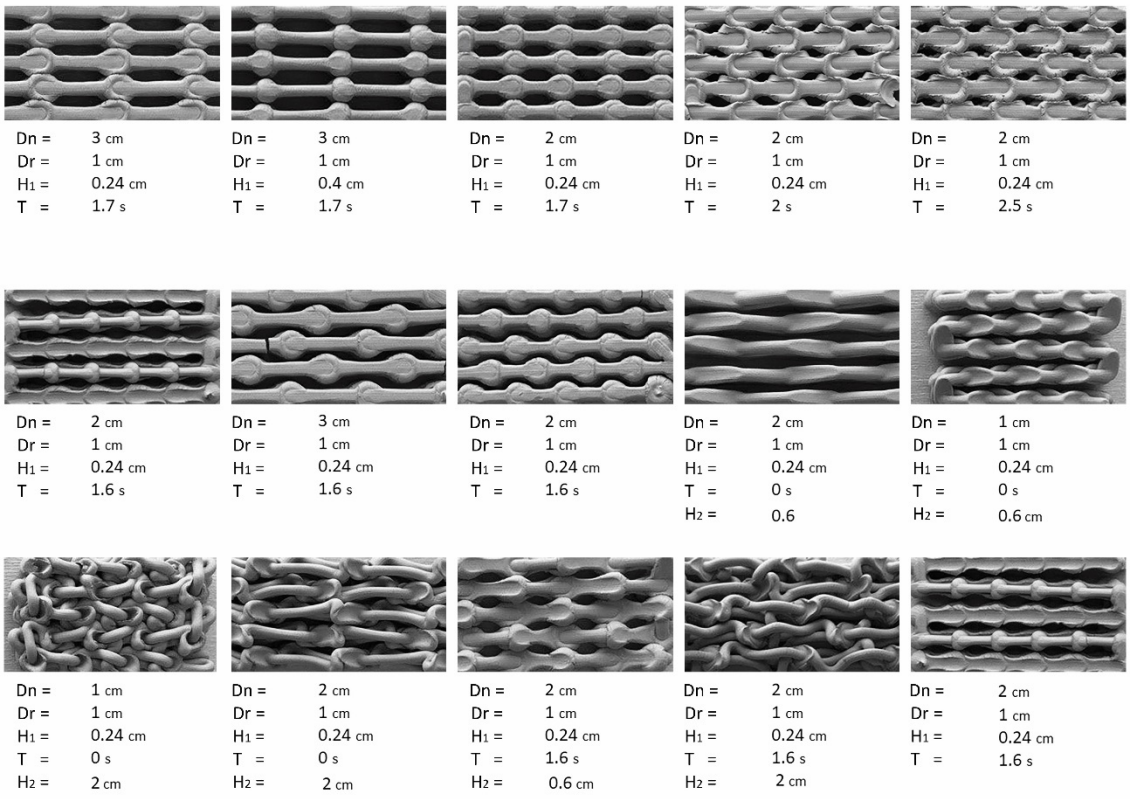

Figure 2.6: Manipulations of process parameters impact geometry during the material deposition process, creating different patterns

While each parameter can span a range of values, applying values beyond a defined interval can cause undesirable irregularities in the printed object (Figure 2.7). For instance, since the interparticle adhesion of the clay is low, when the H_2 parameter is more than 600% of the nozzle diameter, the vertical filament extending from the printer head to the point of application can tear due to the local application of shear. Conversely,

when the H_2 parameter is less than 40% of the nozzle diameter, it results in excessive material deposition along the tool path. This happens because the yield stress of the paste material is low while the pressure at the nozzle tip is high. Therefore, values less than the defined minimum value create a pressure gradient and cause the material to squirt. This will cause material accumulation around the nozzle, and when it continues along the tool path, it will decrease the accuracy of material deposition and result in failure of the print process. That means the H_2 parameter is limited to 40% of the nozzle diameter $< H_2 <$ 600% of the nozzle diameter.

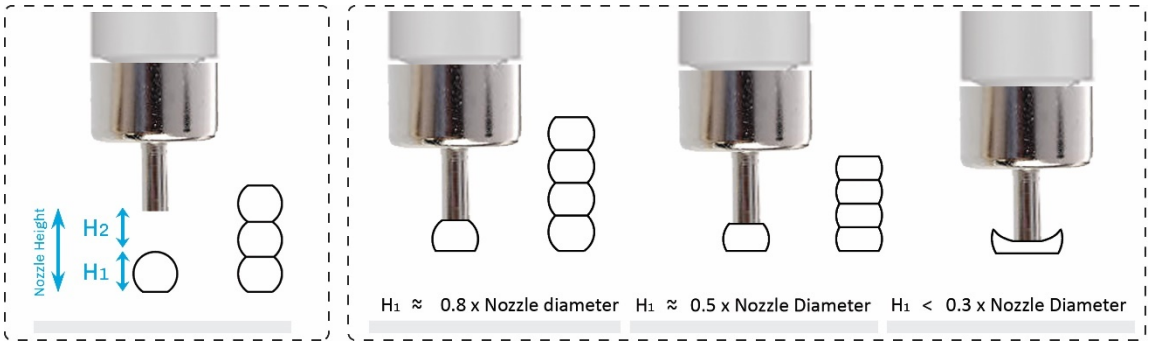

Figure 2.7: Schematic boundary of the H_1 and H_2 parameters

2.4.3. Digital Reconstruction

The third step is reconstructing a digital 3D model from the printed objects (Figure 2.8). The main challenge here is that initial digital models generated in the software are not adequate for reliable analysis since they lack the impacts of the environmental factors as discussed in the previous step. Accordingly, the digital reconstruction step that includes X-ray CT scanning, digital image processing, and 3D

reconstruction was developed to attach secondary geometric characteristics to the initial digital model.

Figure 2.8: Physical specimens printed at the lab before the 3D reconstruction step

2.4.3.1. Scanning

There are several techniques for creating a visual representation of an object. While techniques such as photogrammetry utilize photographs to visualize the outer surface of an object, other imaging modalities such as X-ray CT scanning and magnetic resonance imaging (MRI) use X-ray, magnetic fields, and radio waves to produce more detailed, cross-sectional images of both the inner and outer contours of an object (Kalender 2011). X-ray CT scan technology was used for the 3D reconstruction of the printed objects to create a detailed visualization of each specimen. The outcome of the X-ray CT scanning is a series of 2D images and almost 1,100 gray-scale images for each specimen in this paper, which were used to create voxel-based 3D models. The axial

resolution of the scan (slice thickness) was set to 0.245 mm to create high-resolution images. As a granular material, table sugar was used to improve the accuracy of the scan process and provide a transition from a low-density environment (air) into a dense material (clay) (Figure 2.9).

Figure 2.9: Preparing specimens for X-ray CT scanning. As a granular material, table sugar facilitated the transition from a low-density environment into a dense one to increase the accuracy of the scan

2.4.3.2. Digital image processing

An algorithm was developed in Python to extract the object from the 2D images. The algorithm used image segmentation techniques to create a mask that includes the printed object in each image based on a given threshold. In other words, the created mask contains only those pixels of the gray-scale image with a brightness value in the range of the given threshold.

2.4.3.3. 3D reconstruction

Ultimately, a 3D mesh of each specimen was calculated from the defined mask. Each pixel of the 2D image in the segmentation step defines a cube in a 3D space called a voxel. The models in this paper had a voxel size of (x/y/z) 0.254/0.254/0.254 mm. The

method of creating a polygon mesh from a voxel-based geometry has been explained by Brown et al. (2019) and will be briefly described here. The voxel to mesh conversion algorithm calculates whether a triangular surface passes through a voxel or not. This procedure is also known as the “Marching Cubes” algorithm, where it creates a triangular surface for a 3D model.

Since finite element analysis (FEA), a numerical method for analyzing engineering and mathematical modeling, was performed in this paper, the reconstructed mesh models should be optimized for the analysis step. The triangular surfaces created in this step were slightly modified to fix small inclusions, inverted normals, small gaps, and unconnected and intersecting triangles. Those modifications were necessary toward the FEA, where an enveloping surface is required.

2.4.3.4. Analysis

What is significant about the final step is the emphasis of the workflow on evaluating the bond strength between layers and creating a library based on the patterns created in the previous steps. COMSOL Multiphysics (COMSOL Inc. 2020), a finite element analysis software, was used for numerical simulations and the final analysis (Figure 2.10).

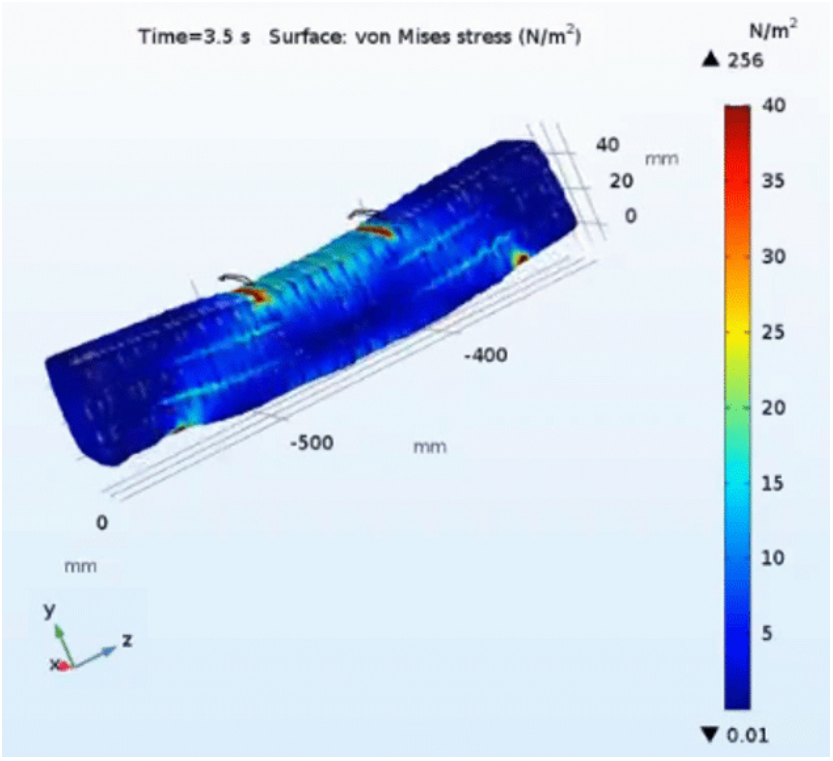

Figure 2.10: COMSOL Multiphysics, a finite element analysis software, was used for numerical simulations and the final analysis

While the research objective was to assess the bond strength between layers, the shear force was the most important area for the investigation. The flexural strength test of concrete and mortar was adopted to evaluate each pattern. The primary test was the standard test method of ASTM C78 (concrete) and C580 (mortar) (ASTM International 2013) that specifies the modulus of rupture in MPa (Figure 2.11).

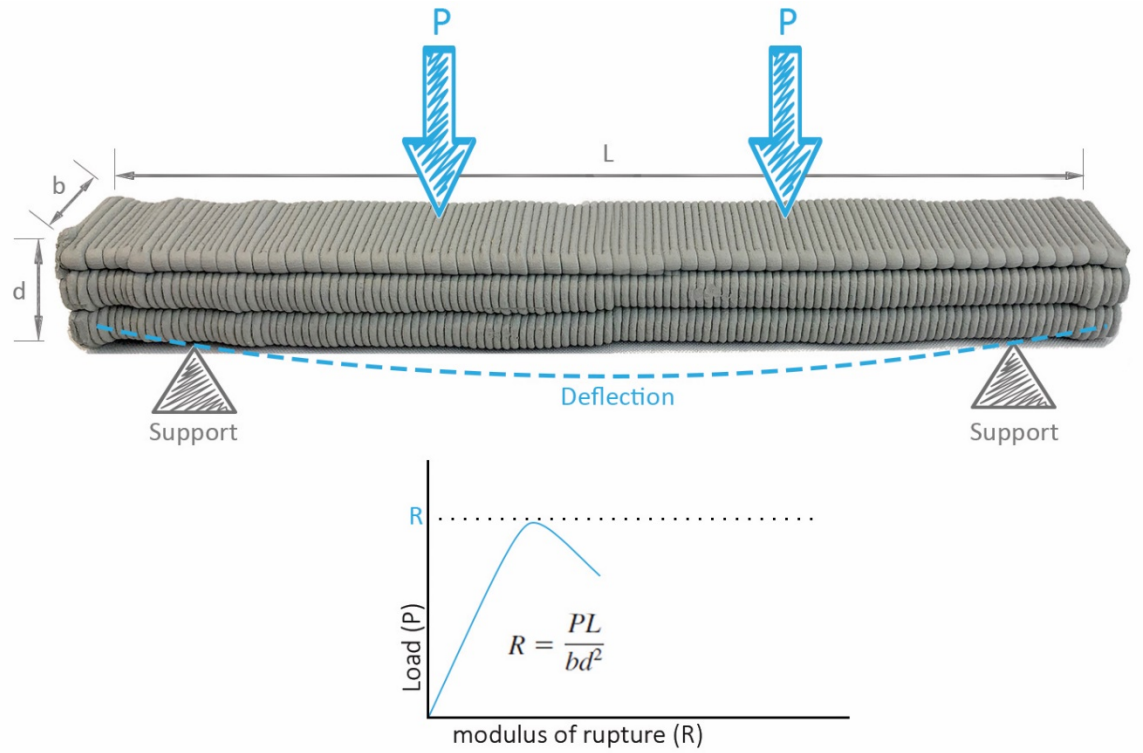

R = modulus of rupture, MPa [psi]
P = maximum applied load indicated by the testing machine, N [lbf]
L = span length, mm [in.]
b = average width of specimen, at the fracture, mm [in.]
d = average depth of specimen, at the fracture, mm [in.]

Figure 2.11: Customized flexural test, ASTM C78 and C580, to evaluate the bond strength between layers of paste in AM

The flexural test was simulated in COMSOL to evaluate the bond strength between layers for the 3D reconstructed models. The four-point load condition was simulated, and associated load boundaries were applied to the 3D mesh models. Simulating point forces are possible in COMSOL, where a force is applied to a single point on the surface of the geometry, although point forces do not exist in the real world and result in infinite stresses in theory. In the digital analysis step in this paper, forces

are distributed over small patches on the mesh surface instead to simulate what happens in the physical flexural test in the lab.

The test provides values for the modulus of rupture for each pattern applied to the specimens.

$$R = P*D_n / b*d^2$$

P is the maximum force applied, D_n is the length of the specimen, *b* is the specimen's width, and d represents the depth of the specimen. Higher modulus rupture values reflect better bond strength between layers. Each pattern was evaluated based on the given constraints, and a library was created accordingly for use in future research (Figure 2.12).

2.4.3.5. Additional Step

One question remains to be answered: To what extent are the results of the analysis close to reality? Although digital modeling, simulation, and analysis have made it faster and easier to design and make predictions about the results for an architectural fabrication, the accuracy of those predictions needs to be evaluated and generalized for future applications. A series of physical tests were designed based on the four-point flexural strength test to calibrate and evaluate the reliability of the proposed workflow. The various patterns resulting from the three selected process parameters' manipulations were applied to a 2 in × 2 in × 11 in beam-shape geometry to evaluate the bond strength between layers. All the samples were robotically 3D printed with clay and were used in

the physical tests. The comparison between digital and physical tests confirmed, with a small margin of error, the reliability of the workflow.

Figure 2.12: The proposed pattern library to be used by an architect or an AI algorithm based on architectural forms and structural requirements

2.5. Discussion

Extant research on improving structural features and expanding architectural applications of large-scale AM processes address different scales of the topic. There is no doubt that paste materials, due to their flexibility, have plenty of potential for creating architectural free forms. However, some issues in using paste materials in AM processes, such as cold joints, reinforcement, and aesthetics, need to be taken into consideration. They can be addressed through approaches such as material optimization at the micro scale, and geometrical considerations in design, form optimization, etc., at the meso and macro scales. The binding between layers in AM can be improved at both the micro and meso scales. The authors have offered a geometric solution for the issue by involving the selected process parameters in the design process. It is worth mentioning that the proposed workflow offers a pattern library, not just a final or ultimate pattern. There is no single best pattern. Rather, there can be an optimum choice that an architect or an AI algorithm can choose based on the given geometry and applied forces. For example, in a surface with dominant shear forces, an optimum pattern would be different from a vertical surface at the corner of a form, where compression forces are most influential.

2.6. Conclusion

The main objective of this chapter was to investigate the structural integrity of an AM process on a meso scale through manipulations of process parameters. A novel workflow was presented to include process parameters in the design process and introduce a digital analysis procedure for robotic-assisted AM with paste. In addition to X-ray scanning, image processing techniques were employed to scrutinize the impacts of environmental stimuli on the printed objects and reconstruct the digital model. The impacts of manipulations of the three selected process parameters on binding between layers were digitally analyzed, and they indicated that these manipulations did improve the bond strength between layers in AM with paste. Finally, a pattern library was offered for use in robotic-assisted AM processes with paste.

2.7. References

ASTM International. 2013. “F2792-12a - Standard Terminology for Additive Manufacturing Technologies.” Rapid Manufacturing Association. West Conshohocken, PA. https://doi.org/10.1520/F2792-12A.2.

Bajpayee, Aayushi, Mehdi Farahbakhsh, Umme Zakira, Aditi Pandey, Lena Abu Ennab, Zofia Rybkowski, Manish Kumar Dixit, et al. 2020. “In Situ Resource Utilization and Reconfiguration of Soils into Construction Materials for the Additive Manufacturing of Buildings.” Frontiers in Materials 7 (March): 1–12. https://doi.org/10.3389/fmats.2020.00052.

Bhardwaj, Abhinav, Scott Z Jones, Negar Kalantar, Zhijian Pei, John Vickers, Timothy Wangler, Pablo Zavattieri, and Na Zou. 2019. “Additive Manufacturing Processes for Infrastructure Construction: A Review.” Journal of Manufacturing Science and Engineering 141 (9). https://doi.org/10.1115/1.4044106.

Bos, Freek, Rob Wolfs, Zeeshan Ahmed, and Theo Salet. 2016. “Additive Manufacturing of Concrete in Construction: Potentials and Challenges of 3D Concrete Printing.” Virtual and Physical Prototyping 11 (3): 209–25. https://doi.org/10.1080/17452759.2016.1209867.

Brown, Justin L, Takuya Furuta, and Wesley E Bolch. 2019. “A Robust Algorithm for Voxel-to-Polygon Mesh Phantom Conversion.” In Brain and Human Body Modeling: Computational Human Modeling at EMBC 2018, edited by Sergey Makarov, Marc Horner, and Gregory Noetscher, 317–27. Cham: Springer International Publishing. https://doi.org/10.1007/978-3-030-21293-3_17.

Buchanan, C., and L. Gardner. 2019. “Metal 3D Printing in Construction: A Review of Methods, Research, Applications, Opportunities and Challenges.” Engineering Structures 180: 332–48. https://doi.org/10.1016/j.engstruct.2018.11.045.

Buswell, R. A., W R Leal De Silva, S. Z. Jones, J. Dirrenberger, W. R. Leal de Silva, S. Z. Jones, and J. Dirrenberger. 2018. “3D Printing Using Concrete Extrusion: A Roadmap for Research.” Cement and Concrete Research 112 (October 2017): 37–49. https://doi.org/10.1016/j.cemconres.2018.05.006.

Buswell, R. A., R. C. Soar, A. G F Gibb, and A. Thorpe. 2007. “Freeform Construction: Mega-Scale Rapid Manufacturing for Construction.” Automation in Construction 16 (2): 224–31. https://doi.org/10.1016/j.autcon.2006.05.002.

Cesaretti, Giovanni, Enrico Dini, Xavier De Kestelier, Valentina Colla, and Laurent Pambaguian. 2014. “Building Components for an Outpost on the Lunar Soil by Means of a Novel 3D Printing Technology.” Acta Astronautica 93: 430–50. https://doi.org/10.1016/j.actaastro.2013.07.034.

Gosselin, C., R. Duballet, Ph Roux, N. Gaudillière, J. Dirrenberger, and Ph Morel. 2016. “Large-Scale 3D Printing of Ultra-High Performance Concrete - a New Processing Route for Architects and Builders.” Materials and Design 100: 102–9. https://doi.org/10.1016/j.matdes.2016.03.097.

Guo, Nannan, and Ming C. Leu. 2013. “Additive Manufacturing: Technology, Applications and Research Needs.” Frontiers of Mechanical Engineering 8 (3): 215–43. https://doi.org/10.1007/s11465-013-0248-8.

Kalender, Willi A. 2011. Computed Tomography: Fundamentals, System Technology, Image Quality, Applications. Erlangen: Publicis.

Khoshnevis, Behrokh. 2004. “Automated Construction by Contour Crafting, Related Robotics and Information Technologies.” Automation in Construction 13: 5–19. https://doi.org/10.1016/j.autcon.2003.08.012.

Wangler, Timothy, Ena Lloret, Lex Reiter, Norman Hack, Fabio Gramazio, Matthias Kohler, Mathias Bernhard, et al. 2016. “Digital Concrete: Opportunities and Challenges.” RILEM Technical Letters 1: 67–75. https://doi.org/10.21809/rilemtechlett.2016.16.

Zareiyan, Babak, and Behrokh Khoshnevis. 2017. “Interlayer Adhesion and Strength of Structures in Contour Crafting - Effects of Aggregate Size, Extrusion Rate, and Layer Thickness.” Automation in Construction 81: 112–21. https://doi.org/10.1016/j.autcon.2017.06.013.

The first article in the series focused on the development of a workflow that outlined the required steps to design, fabricate the specimens, and evaluate the impact of the three selected process parameters on interlayer bond strength in paste AM.

The following chapter details the methodology of the research and discusses the equipment, material, and physical tests used in the study, as well as the test results and findings.

3. IMPACT OF THREE ROBOTIC 3D PRINTING PROCESS PARAMETERS ON INTERLAYER BOND STRENGTH

3.1. Overview

While large-scale Additive Manufacturing (AM), often known as 3D printing, appears to be a viable method for constructing architectural forms and structures, several researchers aim to address the issues related to the layer-to-layer nature of printed elements. One of the susceptible areas in this technology is the bond strength between layers. The current paper seeks to expand upon the knowledge about the impact of three process parameters (Dn, the distance between hypothetical nodes on the toolpath, H_2, the standoff distance of the nozzle, T, the delay time at each point) on interlayer bond strength in paste AM, since it provides a foundation for large-scale free form architectural fabrication. Furthermore, concerns about global carbon emissions associated with the concrete industry prompted the authors to consider replacing concrete with a clay-based material in large-scale AM. This paper proposes a technical approach by manipulating process parameters that alter the geometry of the layers on the meso-scale to emulate densification and to enhance friction between consecutive layers in robotically assisted AM with paste.

Difficulties associated with simulation and prediction of finite element analysis approach have been discussed, and the standard flexural test was adopted to evaluate and analyze 95 printed specimens. According to the findings of the flexural tests, periodically manipulating the H_2 parameter based on the given criteria served as

compaction in conventional concrete casting methods and improved the interlayer bond strength under shear by 41.2% on average. Due to the inconsistency of the findings, however, it was not possible to detect any obvious impact of the T parameter on interlayer bond strength.

3.2. Introduction

The low productivity in the construction industry, in contrast to automated sectors such as the automotive industry and the increase in shortages of skilled laborers, has been a source of concern in the last decade (Schutter et al. 2018). The deliberate digitalization and automation of all relevant phases, from planning and design to the final construction process, appear necessary. Large-scale Additive Manufacturing (AM) is a burgeoning area of technology that has garnered considerable attention from both the construction industry and academics worldwide.

Concrete and cement-based materials are at the core of attention in the large-scale AM industry because of their availability, extrudability, affordability, customizable setting time, and significant mechanical properties (Khan et al. 2020; Paolini et al. 2019; Schutter and Lesage 2018; Wangler et al. 2016). The concrete industry, however, is responsible for 5-8% of global carbon emissions (IEA 2019). It is crucial to replace concrete with a more sustainable material along with technological breakthroughs in the construction industry. Cement substitutes such as fly ash, a blast furnace byproduct, have decreased the average CO_2 footprint of the concrete industry, but the emission is still significant (Uliasz-Bocheńczyk and Mokrzycki 2020). Bos et al. (2016) brought up the

fact that the lack of economic motivation due to the use of cheap raw materials in the concrete mix makes it difficult to reduce concrete-related CO_2 emissions. In situ resource utilization is one approach to decrease the CO_2 footprint of large-scale AM. Minerals available in the Earth's crust, however, form a naturally sourced material palette that has been used throughout history and can be used in modern technologies such as large-scale AM (Bajpayee et al. 2020). Concrete has remarkable compressive strength and it is difficult, but not impossible, to completely replace it with a clay-based material and achieve similar mechanical properties. Bajpayee et al. (2020) proposed to harvest local materials, such as ordinary backyard soil, to configure an extrudable material compatible with large-scale AM processes. The authors' approach is intended to decrease transportation costs, embodied energy in building materials, and CO_2 emissions.

It is important to understand that material, design, process, and product all have a tight connection in AM with paste. Layer-to-layer interface is the inherent nature of 3D printed elements. A substrate (the deposited layer) should be hard enough to hold its shape, carry the load of upper layers and be soft enough to adhere to overlays (new layers). The mechanical properties of the interfaces depend on chemical and physical states as well as the rheological and morphological features of both the substrate and the overlay (Khan et al. 2020; Nerella et al. 2019). While the bond strength between layers is considered the "Achilles' heel" of 3D printed elements produced by extrusion-based material deposition, several researchers investigated the issue on both meso- and micro-

scales (Keita et al. 2019; Lu et al. 2021; Marchment et al. 2017; Marchment and Sanjayan 2019; Nerella et al. 2019; Nerella and Mechtcherine 2017; Panda et al. 2019; Sanjayan et al. 2018; Santos et al. 2012). This paper is part of a more extensive study that introduces three scales in extrusion-based large-scale AM process: micro-, meso-, and macro-, which are responsible for material properties, interlayer adhesion, and the geometry of architectural forms, respectively (Bajpayee et al. 2020; Farahbakhsh et al. 2020).

Densification plays a crucial role in paste AM processes. According to Bos et al. (2018) the quality of the layer interface and bond strength in paste AM processes depends not only on the chemical reactions in material, but also substantially on the physical compaction. Vibration and self-compacting materials have been used in ordinary concrete applications to enable the physical intermixing of concrete layers and achieve compaction. Per Hoornahad (2015), however, neither is possible in paste and concrete 3D printing processes because of the layered nature of printed objects. They stated that self-compaction and zero-slump are mutually exclusive goals that can only be partially met at the same time.

Several approaches in the literature seek to improve the mechanical performance of consecutive layers in paste 3D printing. Those approaches aim at addressing the risk of cold joint formation on meso- and micro-scales.

3.2.1. Micro-scale

At the micro-scale, chemical interactions are responsible for the adhesion between layers. Several research groups attempted to address the absence of a cohesive chemical bond between successive layers in paste AM. Nerella et al. (2019) studied the influence of binder composition on the mechanical performance of 3D printed concrete elements where they used two different mixtures, one with and the other without pozzolanic additives. Verian et al. (2018) suggested spraying a primer (a chemical that is meant to increase the adhesion between consecutive layers) on the substrate just before depositing the overlay.

Similarly, in another study, a second substance (a polymer containing sulfur and black carbon) was used as an adhesive between consecutive layers (Hosseini et al. 2019). The researchers reported greater bond strength compared to ordinary 3D printing procedures. Marchant et al. (2019) proposed a method for creating a mechanical anchoring effect. They claimed that adding a cementitious paste to the top of the substrate before the deposition of the overlay would result in greater interlayer bond strength.

While the interlayer interval time has a correlation with the surface moisture condition of the substrate, previous research has shown that the surface moisture content plays a crucial role in the interlayer adhesion. The moisture content depends on the bleed rate of the concrete (a phenomenon in which free water in the mix climbs up to the surface) and the rate of losing moisture from the surface (owing to evaporation and

chemical reaction) (Marchment et al. 2017; Sanjayan et al. 2018). They concluded that the higher the moisture content on the substrate surface, the stronger the interlayer adhesion.

3.2.2. Meso-scale

On the Meso-scale, process parameters and layer configurations affect the interlayer bond strength. The time gap for printing successive layers increases with printing larger structures and multi-session processes. Several researchers studied the effect of interlayer interval time on the bond strength (Le et al. 2012; Nerella and Mechtcherine 2017; Panda et al. 2018; Wolfs et al. 2019; Zareiyan and Khoshnevis 2017b). They reported that the bond strength between successive layers has an inverse correlation with interlayer interval time.

There are some studies on the effect of the nozzle height (the distance between the nozzle and the print surface, which is referred to as H_2 in this paper) on the bond strength between layers (Panda et al. 2019; Wolfs et al. 2019). The reported results, however, are inconsistent. While one of the studies (Panda et al. 2019) reported that bond strength increases significantly when H_2 decreases, the others did not find any relation between H_2 and the bond strength between layers. This paper has new findings that confirm Panda et al. results and will be discussed in the result section.

Several researchers have reported that compaction and roughness of the substrate enhance the friction with the overlay and, as a result, improves the cohesiveness of the consecutive layers. According to Bos et al. (2016), moderately pressing the nozzle tip

into the overlay can be beneficial to improving the printed product's mechanical properties. The pressure applied to the product by the printer head should help with compaction and interface adherence. Zareyan and Khoshnevis (2017) proposed an interlocking approach to create macroscopic roughness and confirmed its positive impact on interface bond strength of layered specimens. The high kinetic energy of the sprayed material, which helps mitigate the risk of cold joint formation, is claimed to improve layer interlocking and therefore, interlayer bond strength in a process known as Shotcrete 3D Printing (SC3DP) technology (Kloft et al. 2020).

Eight process parameters were identified in a robotic-assisted AM process (Farahbakhsh et al. 2020) and are elaborated upon in a chart (Figure 3.1). Among those, the impacts of three process parameters (Dn, H_2, and T, which are explained in more detail in the next section) on the interlayer bond strength have received less attention in the literature.

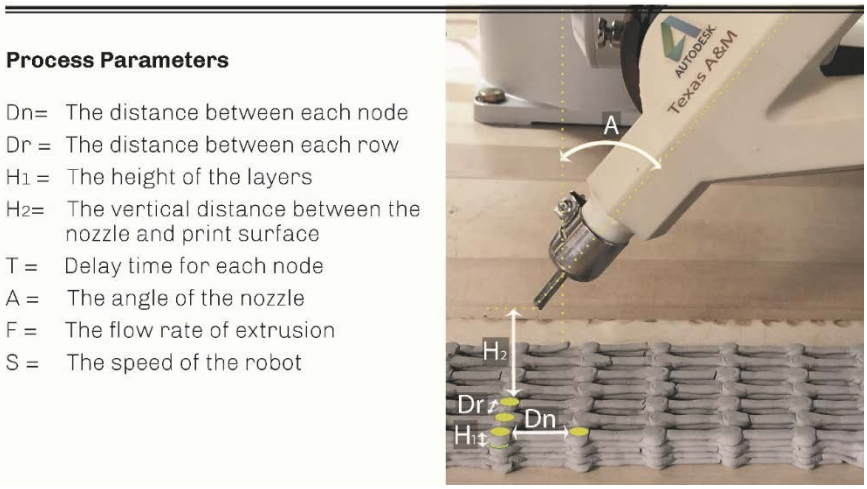

Figure 3.1: Eight process parameters in a robotic-assisted AM process are illustrated in this chart (Farahbakhsh et al. 2020)

This paper proposes a technical approach by manipulating process parameters that alter the geometry of the layers on the meso-scale to emulate densification and to enhance friction between consecutive layers in robotically assisted paste AM processes (Figure 3.2).

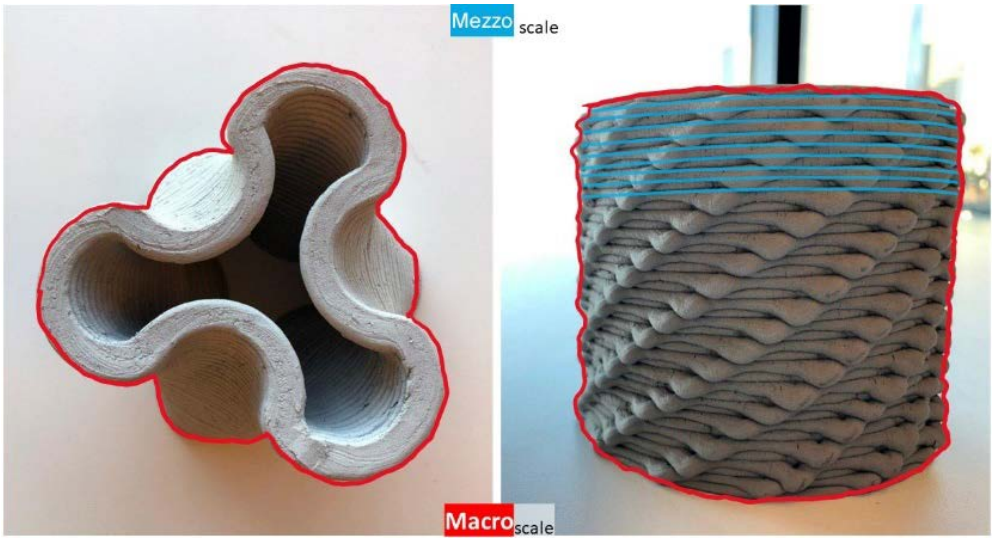

Figure 3.2: Macro- and meso-scale are depicted in this picture. While the meso-scale is related to the layer interfaces, the micro-scale includes the material properties and behaviors

3.3. Method

The surface condition in a paste AM process can be manipulated on both micro- and meso-scales. Theoretically, manipulating the selected process parameters affects the geometry of the substrate's surface at the meso-scale. Therefore, the authors hypothesized that those manipulations would imitate compaction and enhance the friction between the substrate and the overlay. Three selected process parameters were systematically varied in specified intervals, and three specimens were 3D printed for

each parameter change to be assessed in a series of tests developed based on the existing mortar and concrete flexural standard testing (see further discussion below).

3.3.1. Selected Process parameters

3.3.1.1. D_n Parameter

The first process parameter (D_n) investigated in this paper is the distance between hypothetical nodes on the toolpath and depends on the other two parameters. For example, a curve on the toolpath was divided into several segments with the length of D_n, and consequently, at each node on the toolpath there were certain values for H_2 and T.

3.3.1.2. H_2 Parameter

The second process parameter is the standoff distance of the nozzle from the most recent substrate (H_2). Considering the thickness of the paste filament, varying H_2 would create a bumpy surface rather than the flat one that is often observed in most 3D printing processes. This is analogous to pushing the soft overlay material against the semihard substrate on a periodic basis. In the literature, most of the researchers consider a constant value for this parameter when 3D printing the specimens. In order to create a bumpy surface, however, the manipulation of the H_2 parameter should happen in a periodic pattern. When a value was assigned to H_2 in the current study, H_2 was varied in the interval of zero and the given value at every other node (Figure 3.3).

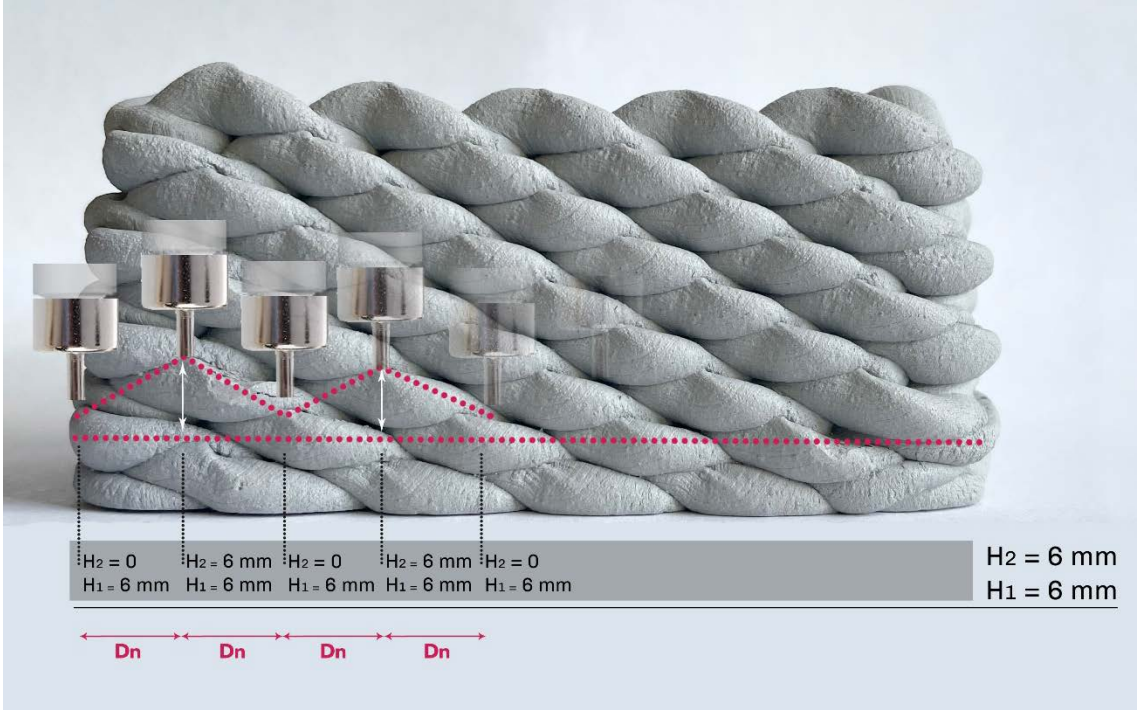

Figure 3.3: The manipulation of the H_2 parameter should happen in a periodic pattern to create a bumpy surface

While keeping the H_2 value in a meaningful range could potentially be beneficial to improving the bond strength, values out of that range can either cause undesired irregularities in the printed object or accumulate extra material around the nozzle, making the print surface messy and decreasing the accuracy of material deposition, which ultimately results in failure of the print process (Farahbakhsh et al. 2020). That is mainly because of the low inter-particle adhesion of the fresh material. When the value of H_2 is more than 600% of the nozzle diameter, it leads to paste filament tears due to the local shear application. Conversely, when the value of H_2 is less than 40% of the nozzle diameter, it results in excessive material deposition along the tool path. The latter happens due to the low yield stress of the paste material, while the pressure at the nozzle

tip is high. A pressure gradient shapes when values less than the defined minimum value are assigned to H_2 and cause the material to squirt (Farahbakhsh et al. 2020). Those limited the value of the H_2 parameter between 40% and 600% of the nozzle diameter in this paper (Figure 3.5).

3.3.1.3. T Parameter

The third process parameter is the delay time (T) that refers to the period that the robot and the printhead attached to it stop moving; still, the material flow and the deposition process continue. This results in more material deposition at the stopping points and potentially creates a larger contact surface between consecutive layers. As with the H_2 parameter, it is critical to maintain T's value within an acceptable range to prevent the print process from failing. The meaningful range of values for T in this study was based on the printhead velocity of 35 mm/s and was limited between 0.6 s to 1.6 s. While delays less than 0.6 s had little or a negligible impact, delays more than 1.6 s resulted in excessive material flow on the print surface, resulting in either undesired finishing or structural collapse due to unequal weight distribution (Farahbakhsh et al. 2020). Therefore, three values, 0.6, 1, and 1.6, were assigned to the T parameter to create specimens for the destructive tests (Figure 3.4 and Figure 3.5).

Figure 3.4: Increased material deposition at the stopping points theoretically enhances the surface contact between successive layers

It is critical to highlight an issue that was expected and observed during the manipulation of both H_2 and *T* parameters. When values higher than the prescribed intervals for H_2 and T and lower values for D_n were applied to the specified process parameters, excessive material buildup occurred. This might decrease the accuracy of the printed product and fail in the process. Softer pastes are more vulnerable to this phenomenon.

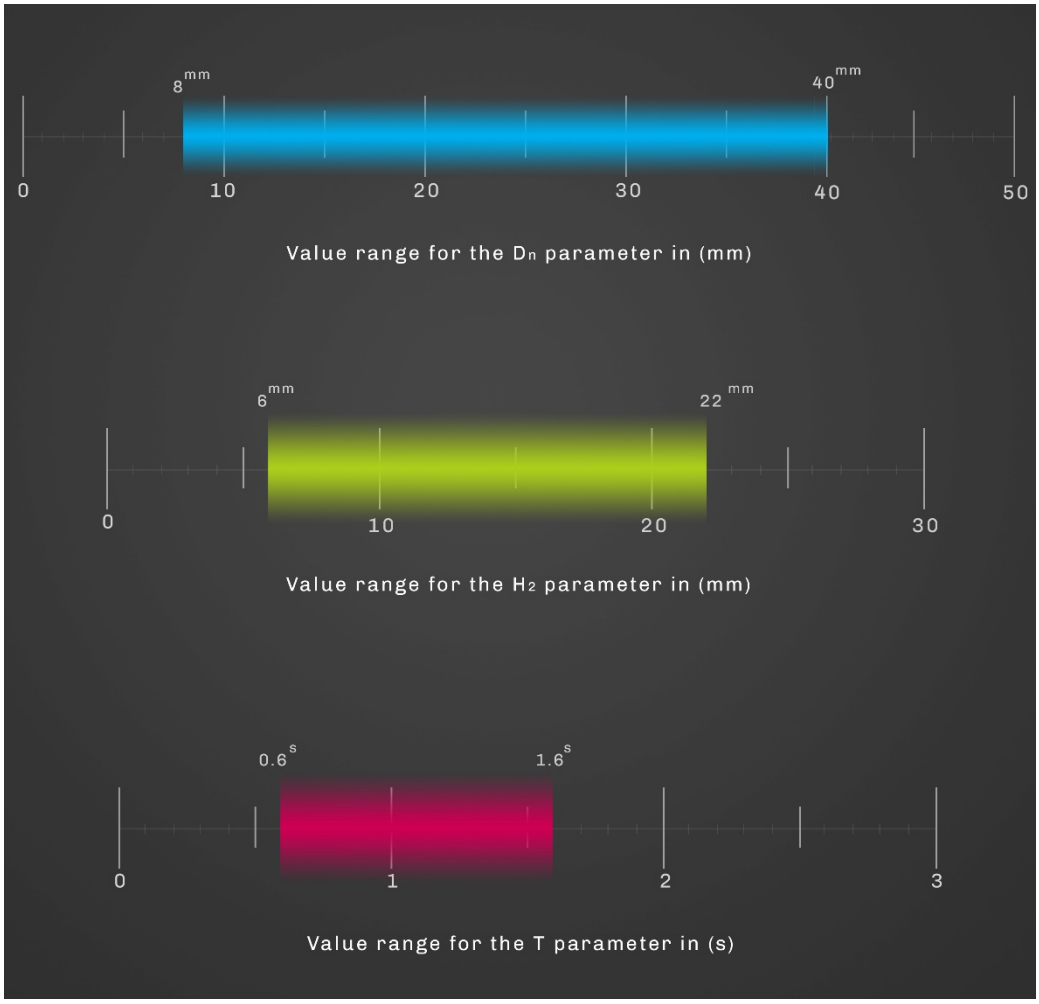

Figure 3.5: Value range for the selected process parameters

3.3.2. Material

While the focus of this paper is the impact of the selected process parameters on the bond strength between layers in paste 3D printing, a comprehensive description of a bespoke clay-based material that was used in this paper is provided in (Bajpayee et al. 2020). The clay-based material contained 32% silt, 30% sand, 23% gravel, 15-18% clay (kaolinite), water, and a stabilizing agent.

3.3.3. Equipment

The material delivery system used in this study comprised a hybrid of a pneumatic and mechanical setup. The material was pushed via a diaphragm sustained by 80 to 125 PSI pneumatic pressure through a hose with 19 mm inner diameter and was delivered to a custom-designed extruder at the printer head. The extruder included an auger, controlled by a microcontroller and driven by a NEMA 23 stepper motor, that created a linear mechanical pressure to supply consistent material at the nozzle tip. The custom-designed extruder was mounted on an ABB IRB 1200 industrial robotic arm. A circular nozzle with 8 mm diameter and 40 mm length was employed for material deposition.

3.3.4. Testing method

To the best of the author's knowledge, there is no standard procedure for testing the interlayer bond strength for paste AM processes. Different methods have been used in the literature. The interlayer bond strength determines the flexural strength when the specimen is loaded parallel to the print direction. In line with other research (Marchment et al. 2017; Nerella et al. 2019; Sanjayan et al. 2018; Weng et al. 2021; Wolfs et al. 2019), the testing procedure was borrowed from the existing mortar and concrete standards and optimized to apply to 3D printed components.

The standard test method of ASTM C78 (concrete) and C580 (mortar) (ASTM International 2013) were adopted to determine the flexural strength for each specimen in MPa. The flexural test (four-point bending test) setup included a free span between two

supports (W) that was equal to (9 ¾”) 246 mm, and the loading was applied on two points with the distance of (3 ¼”) 82 mm in the middle of the span. The maximum load (P) was recorded at the failure of each specimen and used to calculate the flexural strength (R) of the samples (Figure 3.6 and Figure 3.7).

Due to the printing process, the specimens may be viewed as several thin strips overlaying one after another. In extrusion-based 3D printing, the flexural test is directionally dependent on the layer orientation (Feng et al. 2015; Le et al. 2012; Wangler et al. 2019; Wolfs et al. 2019). According to Feng et al. (2015), applying the load in different directions evaluates either the bond strength between layers, the bond strength between strips, or the compressive strength of the bulk material.

When a load is applied in the X direction (Figure 3.6a), the bond strength between strips is measured. When the specimen is loaded in the Y direction (Figure 3.6b), the compressive strength within the bulk material is evaluated. Finally, when a load is applied parallel to the print direction (Z direction), a relatively smooth fracture pattern develops at the interlayer interface, allowing the assessment of the bond strength between layers (Figure 3.6c). In this paper, the printed specimens were loaded parallel to the print direction to evaluate and ensure that the printed object's structural integrity (interlayer bond strength in particular) is sufficient when subjected to lateral forces such as wind, earthquake, etc.

According to the ASTM standard test (ASTM International 2013), each experimental series required at least a minimum of three samples to obtain a reliable

flexural strength value and to eliminate the possible errors. Ninety specimens regarding the manipulation of the selected process parameters, as well as five specimens with conventional layering, were 3D printed to evaluate the interlayer bond strength under shear.

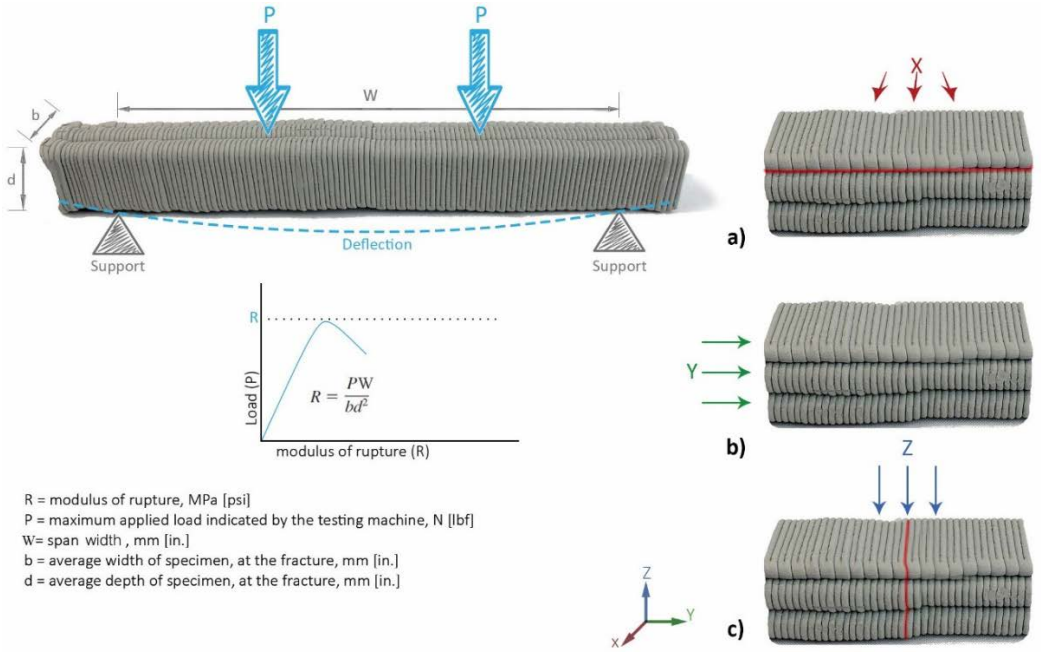

Figure 3.6[9]: The flexural strength of printed specimens was determined via a series of tests (Farahbakhsh et al. 2020). This figure also illustrates the directional dependency of the tests

[9] The original figure of the flexural test from (Farahbakhsh et al. 2020) is modified in this paper. Firstly, the four-point bending test is adopted rather three-point bending test. Secondly, the L symbol is replaced with W to avoid confusion, since L refers to length of the printed specimens.

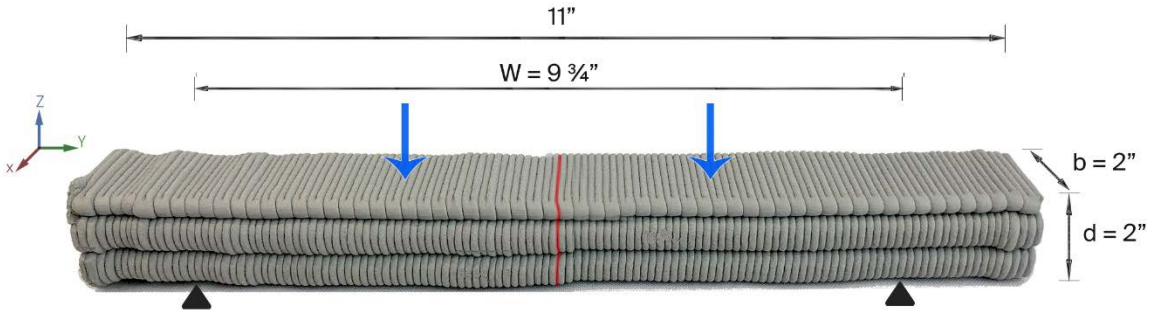

Figure 3.7: The flexural test (four-point bending test) setup

3.4. Results and analysis

All of the specimens in this study were 3D printed based on the required sample size in the ASTM standard flexural test method. The flexural tests were performed on specimens measuring 50.8 mm (2 in) × 50.8 mm (2 in) x 279.4 mm (11 in) with 10% fluctuation due to the layered nature of paste 3D printing. The samples were printed in one continuous process with an interlayer interval time of 30 s.

The mechanical tests were conducted in two groups. In one group (group A), T remained constant while D_n and H_2 were systematically varied. In the other set of experiments (group B), H_2 was kept constant while D_n and T were systematically changed based upon. The flexural strength (R) was calculated using the peak loads from the flexural tests according to:

$$R = P*W / b*d^2$$

Where *P* is the maximum force exerted, *W* is the distance between two supports, here equal to 246 mm, *b* is the specimen's width, and *d* denotes the depth of the specimen (Figure 3.8).

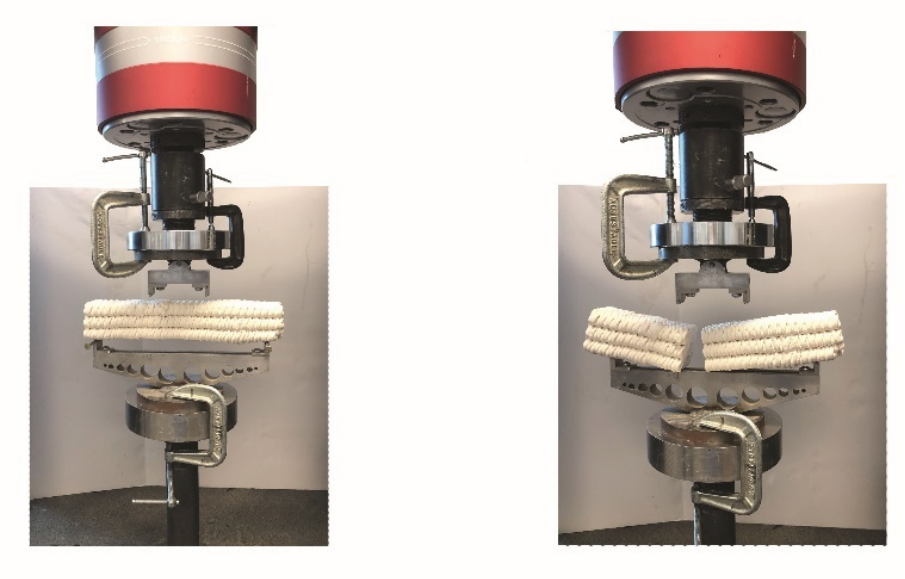

Figure 3.8: Applying the flexural test on the printed specimens

(Table 3.1) and (Table 3.2) present the average flexural strengths for each set of parameters. The full data set can be found in the appendix.

It can be seen that in general, when the H_2 parameter was periodically varied, the flexural strength improved. In contrast, no clear impact of the T parameter on flexural strength was evident since the results are inconsistent.

Table 3.1: In group A, T remained constant while D_n and H_2 were systematically varied

Group A	T (s)	D_n (mm)	H_2 (mm)	R (MPa)
A1-1	0	8	6	3.39
A1-2	0	16	6	3.09
A1-3	0	24	6	3.46
A1-4	0	32	6	3.20
A1-5	0	40	6	3.26
A2-1	0	8	14	3.73
A2-2	0	16	14	3.02
A2-3	0	24	14	3.41
A2-4	0	32	14	3.10
A2-5	0	40	14	3.24
A3-1	0	8	22	3.70
A3-2	0	16	22	3.14
A3-3	0	24	22	3.41
A3-4	0	32	22	3.11
A3-5	0	40	22	3.32

Table 3.2: In group B, H_2 was kept constant while D_n and T were systematically changed

Group B	T (s)	D_n (mm)	H_2 (mm)	R (MPa)
B1-1	0.6	8	0	2.54
B1-2	0.6	16	0	2.37
B1-3	0.6	24	0	2.01
B1-4	0.6	32	0	1.72
B1-5	0.6	40	0	2.33
B2-1	1	8	0	3.13
B2-2	1	16	0	2.80
B2-3	1	24	0	2.21
B2-4	1	32	0	1.85
B2-5	1	40	0	2.83
B3-1*	*The parameter values for this specimen resulted in an excessive accumulation of material and failed to produce an acceptable printed object.			
B3-2	1.6	16	0	2.91
B3-3	1.6	24	0	2.58
B3-4	1.6	32	0	2.36
B3-5	1.6	40	0	2.84

The average bond strength for specimens generated with conventional flat layering was 2.3 MPa for various D_n values, as shown in (Figure 3.9). The percentage change for each series of specimens was calculated using the method below:

(Final Value – Initial Value) / Initial Value * 100

Table 3.3: Flexural strength change as percentage in Group A

Specimens	Flexural strength for the specimens in Group A	Flexural strength for specimens with conventional layering	Percentage change
A1-1	3.39	2.37	**43.04**
A1-2	3.09	2.31	**33.77**
A1-3	3.46	2.34	**47.86**
A1-4	3.20	2.31	**38.53**
A1-5	3.26	2.37	**37.55**
A2-1	3.73	2.37	**57.38**
A2-2	3.02	2.31	**30.74**
A2-3	3.41	2.34	**45.73**
A2-4	3.10	2.31	**34.20**
A2-5	3.24	2.37	**36.71**
A3-1	3.70	2.37	**56.12**
A3-2	3.14	2.31	**35.93**
A3-3	3.41	2.34	**45.73**
A3-4	3.11	2.31	**34.63**
A3-5	3.32	2.37	**40.08**
		Total Average	**41.20**

The average of all results revealed the bond strength improved 41.2% on average when H_2 was periodically varied. The correlation between T and D_n, however, is not clear so far (Figure 3.10).

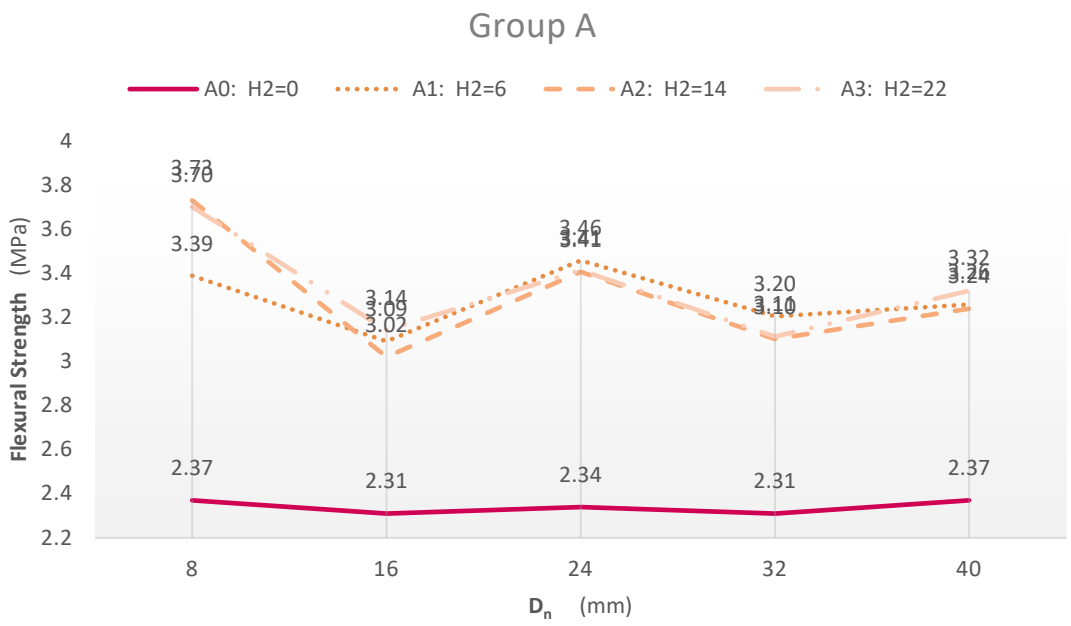

Figure 3.9: Flexural strength of the specimens in Group A

Once the loaded specimen fractured, the fissures propagated suddenly through the entire section, located at the interface of successive layers. In the specimens with conventional layering, the fracture was formed on a flat surface. However, periodically varying H_2 in Group A samples resulted in an uneven cracking surface as depicted in (Figure 3.11b).

In the second study, the *T* parameter's impact was targeted and plotted in (Figure 3.10). It can be seen that the bond strengths have high variability when *T* has been manipulated based on the prescribed range. One explanation might be that achieving an optimum material flow at the nozzle tip for the given *T* values that aim at extending the interlayer surface area is not compatible with the optimum deposition rate on the tool path. Insufficient material flow in a circular nozzle may result in air cavities between

filaments next to each other and weaken the bond strength either between layers, between strips, or both (Figure 3.11c).

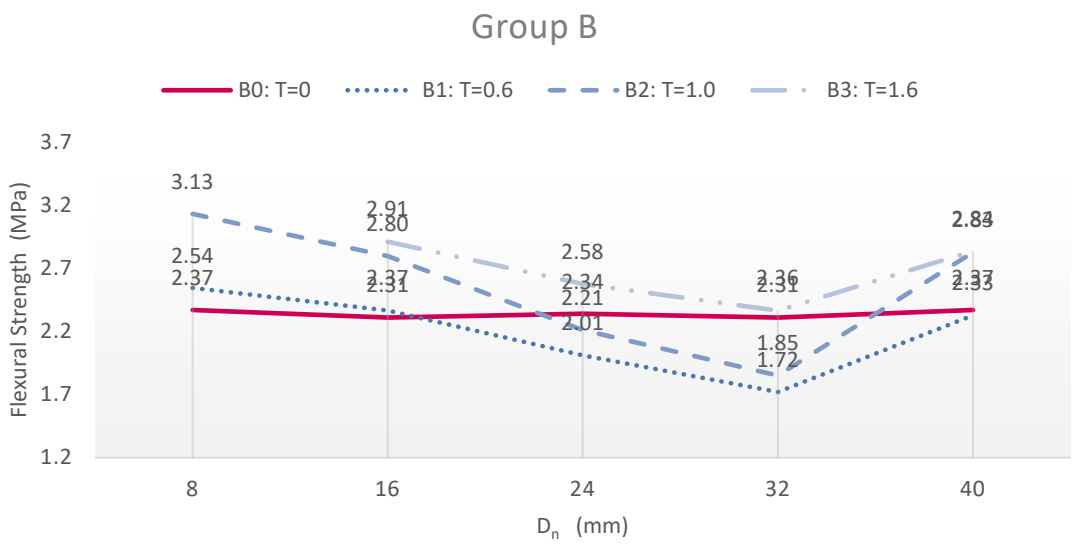

Figure 3.10: Flexural strength of the specimens in Group B

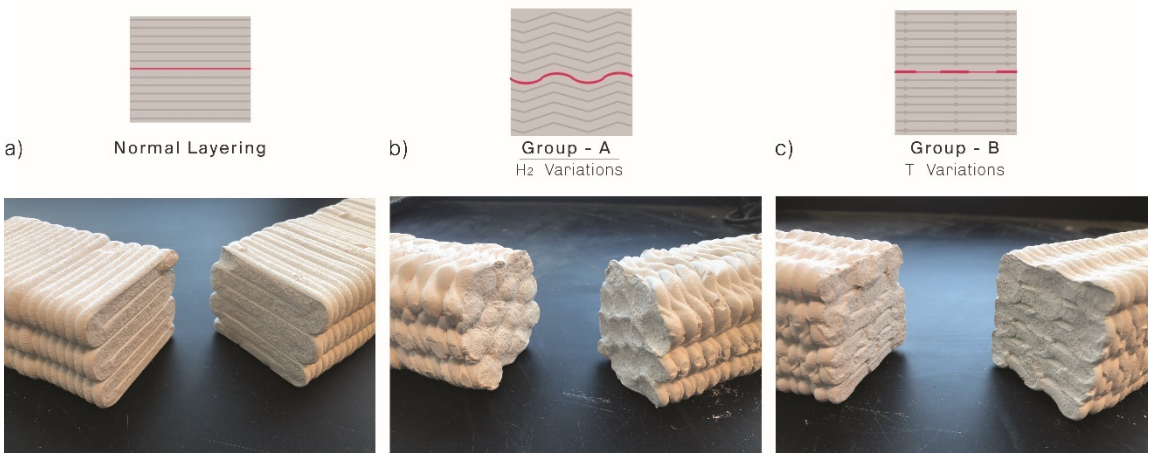

Figure 3.11: Fracture surfaces in three groups of specimens

3.5. Discussion

Several researchers have come up with different results in the literature. These disparities in outcomes might be due to variations in materials, material delivery systems, ambient conditions, and testing methods used in those studies. While Klof et al. (2020) reported a bond strength of 3.7 MPa for extrusion base concrete 3D printing, Le et al. (2012) found an average flexural strength of 7 MPa for the same layer direction for specimens generated with time intervals of 0 minutes and 15 minutes. As prescribed, this paper focuses on studying the impacts of the H_2 and T parameters on the interlayer bond strength in a geometrical context. The process of manipulating the selected process parameters and, as a result, the improved layer binding on the meso-scale were far more intriguing than the highest bond strengths attained in this work.

The effects of the nozzle height on the bond strength between layers have been studied previously, as mentioned in the introduction. On the other hand, the authors investigated the impacts of the H_2 parameter on interlayer bond strength when it was regularly varied between zero and a given value, as shown in (Figure 3.3).

External vibration of already-deposited layers is not recommended because it disrupts structural development (Nerella et al. 2019). In the absence of external vibration in paste AM, varying H_2 on a regular basis not only contributes to the substrate's surface geometry, but also pushes the fresh overlay material into the substrate. It is crucial to clarify that the H_2 parameter in this study is defined as nozzle height (used in previous studies) minus layer height (H_1) (Figure 3.12). It means that the nozzle tip should never

get too close to the substrate's surface since it can cause the material to squirt out. This occurs because while the paste material's yield stress is low, the pressure at the nozzle tip is high. As a result, when the nozzle gets too close to the print surface (closer than 30% of the nozzle diameter), a pressure gradient shapes in the material delivery system, and material squirts out.

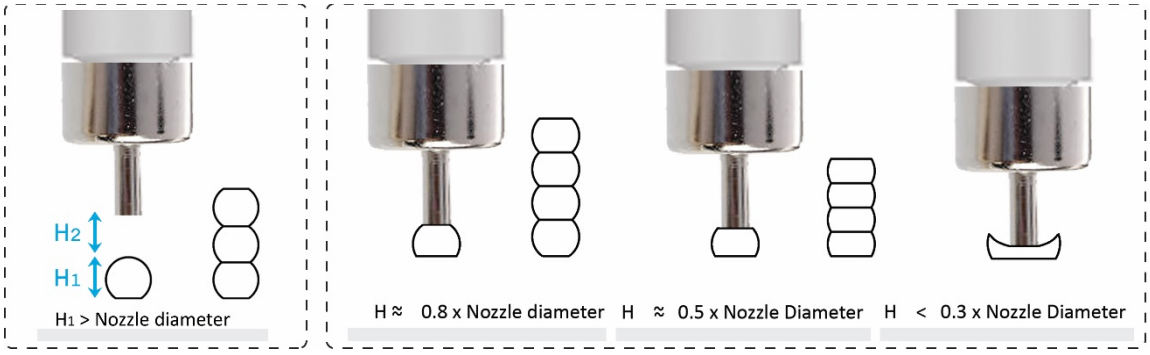

Figure 3.12: Relationship between H_2, H_1, nozzle diameter, and nozzle height

The authors were able to include process parameters in the design phase using the technological approach presented in this study. The print process created a few unique patterns on the print surface as byproducts. While the test results indicated that some level of bond strength enhancement can be accomplished, other patterns may be created based upon as long as the process parameter is varied within the given range. The most interesting finding was the geometrical pattern of layer interfaces during the manipulation of H_2. The increase in the bond strength in Group A of the specimens can be described due to the impact of H_2 on the geometry of the print surface. Following the flexural tests, it became apparent that the diamond-like pattern of the fracture surface

had formed an interlocking feature on the meso scale, which enhanced resistance to shear pressures.

The authors agree with Khan et al. (2020) that using physics-driven models to simulate and predict the whole 3D printing process and printed material performance is not yet accurate, and consequently, data-driven models are in high demand.

3.6. Conclusion

It is vitally important to recognize that design, material, fabrication, environment, and the final product are all interdependent in paste 3D printing. Furthermore, the layered nature of 3D printing makes it more challenging for paste materials since it can cause a possible vulnerability in the printed element known as “cold joints.” The current paper investigated the impacts of three process parameters on the interlayer bond strength in additive manufacturing with a clay-based material within the given ranges as follows:

- **Process parameters:**
    - The distance between hypothetical nodes on the toolpath ($\boldsymbol{D_n}$):

        8 mm, 16 mm, 24 mm, 32 mm, 40 mm
    - The standoff distance of the nozzle from the most recent substrate ($\boldsymbol{H_2}$):

        6 mm, 14 mm, 22 mm
    - The delay time ($\boldsymbol{T}$):

        0.6 s, 1.0 s, 1.6 s
- **Mechanical properties to be evaluated:** flexural strength.

- **Loading directions:** parallel to the print direction

The results of the flexural tests revealed that manipulating the H_2 parameter within the specified range resulted in an average improvement of 41.2% in the interlayer bond strength under shear. So far, however, there has been no discernible effect of the T parameter on bond strength since the findings have been inconsistent.

Following up on the conclusions drawn from both experimental and theoretical approaches, it has been discovered that changing the geometry of the layers interface by manipulating process parameters may alleviate one of the most concerning issues associated with paste 3D printing.

3.7. References

ASTM International. (2013). F2792-12a - Standard Terminology for Additive Manufacturing Technologies. Rapid Manufacturing Association, West Conshohocken, PA.

Bajpayee, A., Farahbakhsh, M., Zakira, U., Pandey, A., Ennab, L. A., Rybkowski, Z., Dixit, M. K., Schwab, P. A., Kalantar, N., Birgisson, B., and Banerjee, S. (2020). "In situ Resource Utilization and Reconfiguration of Soils into Construction Materials for the Additive Manufacturing of Buildings." Frontiers in Materials, 7(March), 1–12.

Bos, F., Wolfs, R., Ahmed, Z., and Salet, T. (2016). "Additive manufacturing of concrete in construction: potentials and challenges of 3D concrete printing." Virtual and Physical Prototyping, Taylor & Francis, 11(3), 209–225.

Farahbakhsh, M., Kalantar, N., and Rybkowski, Z. (2020). "Impact of robotic 3D printing process parameters on bond strength." 40th Annual Conference of the Association for Computer Aided Design in Architecture, ACADIA 2020.

Feng, P., Meng, X., Chen, J. F., and Ye, L. (2015). "Mechanical properties of structures 3D printed with cementitious powders." Construction and Building Materials, Elsevier Ltd, 93, 486–497.

Hoornahad, H., Koenders, E. A. B., and van Breugel, K. (2015). "Towards the development of self-compacting no-slump concrete mixtures." Epitoanyag - Journal of Silicate Based and Composite Materials, 67(4), 135–138.

Hosseini, E., Zakertabrizi, M., Korayem, A. H., and Xu, G. (2019). “A novel method to enhance the interlayer bonding of 3D printing concrete: An experimental and computational investigation.” Cement and Concrete Composites, 99(March), 112–119.

IEA. 2019. “World Energy Outlook 2019.” IEA, Paris. https://www.iea.org/reports/world-energy-outlook-2019.

Keita, E., Bessaies-Bey, H., Zuo, W., Belin, P., and Roussel, N. (2019). “Weak bond strength between successive layers in extrusion-based additive manufacturing: measurement and physical origin.” Cement and Concrete Research, Elsevier, 123(November 2018), 105787.

Khan, M. S., Sanchez, F., and Zhou, H. (2020). “3-D printing of concrete: Beyond horizons.” Cement and Concrete Research, 133(December 2019).

Kloft, H., Krauss, H. W., Hack, N., Herrmann, E., Neudecker, S., Varady, P. A., and Lowke, D. (2020). “Influence of process parameters on the interlayer bond strength of concrete elements additive manufactured by Shotcrete 3D Printing (SC3DP).” Cement and Concrete Research, 134(December 2019).

Le, T. T., Austin, S. A., Lim, S., Buswell, R. A., Law, R., Gibb, A. G. F., and Thorpe, T. (2012). “Hardened properties of high-performance printing concrete.” Cement and Concrete Research, 42(3), 558–566.

Lu, B., Li, M., Wong, T. N., and Qian, S. (2021). “Effect of printing parameters on material distribution in spray-based 3D concrete printing (S-3DCP).” Automation in Construction, 124(February).

Marchment, T., and Sanjayan, J. (2019). Method of enhancing interlayer bond strength in 3D concrete printing. RILEM Bookseries, Springer International Publishing.

Marchment, T., Xia, M., Dodd, E., Sanjayan, J., and Nematollahi, B. (2017). “Effect of delay time on the mechanical properties of extrusion-based 3D printed concrete.” ISARC 2017 - Proceedings of the 34th International Symposium on Automation and Robotics in Construction, (Isarc), 240–245.

Nerella, V. N., Hempel, S., and Mechtcherine, V. (2019). “Effects of layer-interface properties on mechanical performance of concrete elements produced by extrusion-based 3D printing.” Construction and Building Materials, 205, 586–601.

Nerella, V. N., and Mechtcherine, V. (2017). “Micro-and macroscopic investigations on the interface between layers of 3D printed cementitious elements textile reinforced concrete view project SHCC Creep and Durability View project.” (September).

Panda, B., Mohamed, N. A. N., Paul, S. C., Singh, G. V. P. B., Tan, M. J., and Šavija, B. (2019). “The effect of material fresh properties and process parameters on buildability and interlayer adhesion of 3D printed concrete.” Materials, 12(13).

Panda, B., Paul, S. C., Mohamed, N. A. N., Tay, Y. W. D., and Tan, M. J. (2018). “Measurement of tensile bond strength of 3D printed geopolymer mortar.” Measurement: Journal of the International Measurement Confederation, 113(April 2017), 108–116.

Paolini, A., Kollmannsberger, S., and Rank, E. (2019). “Additive manufacturing in construction: A review on processes, applications, and digital planning methods.” Additive Manufacturing, Elsevier, 30(July), 100894.

Sanjayan, J. G., Nematollahi, B., Xia, M., and Marchment, T. (2018). “Effect of surface moisture on inter-layer strength of 3D printed concrete.” Construction and Building Materials, Elsevier Ltd, 172, 468–475.

Santos, D. S., Santos, P. M. D., and Dias-Da-Costa, D. (2012). “Effect of surface preparation and bonding agent on the concrete-to-concrete interface strength.” Construction and Building Materials, Elsevier Ltd, 37, 102–110.

Schutter, G., Lesage, K., Mechtcherine, V., Nerella, V. N., Habert, G., and Agusti-Juan, I. (2018). “Vision of 3D printing with concrete — Technical, economic and environmental potentials.” Cement and Concrete Research, Elsevier, 112(August), 25–36.

Schutter, G., and Lesage, K. (2018). “Active control of properties of concrete: a (p)review.” Materials and Structures/Materiaux et Constructions, Springer Netherlands, 51(5), 1–16.

Uliasz-Bocheńczyk, A., and Mokrzycki, E. (2020). “The potential of FBC fly ashes to reduce CO_2 emissions.” Scientific Reports, 1–9.

Verian, K. P., Carli, M. D., Bright, R. P., and Maandi, E. (2018). “Research Development in 3DCP: Cured-on-Demand with Adhesion Enhancement Delivery System.” Construction and Building Materials, 18(1), 311–319.

Wangler, T., Lloret, E., Reiter, L., Hack, N., Gramazio, F., Kohler, M., Bernhard, M., Dillenburger, B., Buchli, J., Roussel, N., and Flatt, R. (2016). “Digital Concrete: Opportunities and Challenges.” RILEM Technical Letters, 1, 67.

Wangler, T., Roussel, N., Bos, F. P., Salet, T. A. M., and Flatt, R. J. (2019). “Digital Concrete: A Review.” Cement and Concrete Research, 123(June).

Weng, Y., Li, M., Wong, T. N., and Tan, M. J. (2021). “Synchronized concrete and bonding agent deposition system for interlayer bond strength enhancement in 3D concrete printing.” Automation in Construction, Elsevier B.V., 123(December 2020), 103546.

Wolfs, R. J. M., Bos, F. P., and Salet, T. A. M. (2019). “Hardened properties of 3D printed concrete: The influence of process parameters on interlayer adhesion.” Cement and Concrete Research, Elsevier, 119(January), 132–140.

Zareiyan, B., and Khoshnevis, B. (2017). “Interlayer adhesion and strength of structures in Contour Crafting - Effects of aggregate size, extrusion rate, and layer thickness.” Automation in Construction, 81(June), 112–121.

The studies provided in chapters two and three addressed the dissertation's initial research question, which concerned interlayer bond strength in paste AM at meso-scale. The third paper in the following chapter was presented and published at the *CAAD Futures 2021 Conference* hosted by the University of Southern California. The focus of the following paper is on the macro-scale and this question serves as the primary theme: “How a new architectural aesthetic may emerge from robotically assisted additive manufacturing.”

4. PRINT IN PRINT: A NESTED ROBOTIC FABRICATION STRATEGY FOR 3D PRINTING DISSOLVABLE FORMWORK OF A STACKABLE COLUMN

4.1. Overview

In this paper, the fundamentals of a 3D nested construction method for 3D printing stackable tower-like structures are explained, taking into consideration the transportation, storage, assembly, and even disassembly of building components. The proposed method is called "PRINT in PRINT." This paper also documents the authors' experience of and findings from designing and printing a column erected out of a series of 3D printed components in a short stack. Employing the design principles of 3D printing in a nested fashion, the authors showcase the main parameters involved in dividing the column’s global geometry into stackable components. By converting formal, technical, and material restrictions of a robotic-assisted 3D printing process into geometric constraints, the paper describes how the column components are divided, namely that one component shapes the adjacent one.

4.2. Introduction

In recent decades, architects have witnessed and facilitated the emergence of new tools for digital fabrication to bridge the gap between design and fabrication. While the relationship between conception and production has evolved significantly, there is still a considerable gap between what we can draw and what we can build. At this point, the process of fabricating a complex architectural form is relatively expensive and time-consuming and often wasteful. Digital fabrication in architecture is evolving from

building artifacts towards the construction of full-scale buildings. The size of available tools, however, remains a challenge to the integration of digital technologies within construction processes. In recent years, the implementation of larger tools into mainstream construction has made significant contributions. Although employing large tools has great relevance and value for some projects, it can prevent architects from benefiting from the affordability, ease of use, and accuracy of digital fabrication technologies.

While robotic fabrication technologies have enabled the building industry to produce nonstandard architectural forms, the robot's reach and freedom of movement in the space have remained challenging, affecting the size of the final product. Solutions such as cable robots (Izard et al. 2017), gantry systems (Khoshnevis 2004), telescopic booms (Keating et al. 2017), 6-axis robotic arms equipped with external axis (Zhang et al. 2018) have been developed to address the issue. The size of the final product, however, is still limited to the size of the employed robot. For instance, ICON, a 3D printing company in the US, is using a 3-axis gantry solution. Their latest 3D printer can print objects up to 15.5 feet tall (“ICON” 2021). To print an object larger than the actual robot, it is possible to add linear rails that permit the robot to move forward or upward. For instance, in an experimental project called Casa Covida, Emerging Objects, a California-based architectural practice, used a 3-axis lightweight printer to construct structures larger than itself while adding an external fourth axis to lift the printer in the Z direction (Rael and San Fratello 2021).

In this paper, the main objective is to leverage robots to enhance both the sustainability and efficiency of large-scale construction and maintain a consistent relationship between architectural expressions and making. Therefore, we propose a nested 3D printing strategy as a novel method in large-scale robotic fabrication to address the limited height of geometries per the current approaches in the literature (Craveiro et al. 2019).

4.3. Methods

Nesting is not a new concept in the manufacturing industry. It is used to minimize waste and maximize efficiency. The nesting strategy, however, has often been referred to as cutting or shaping patterns on a flat surface (Nee et al. 1986). Here, we proposed a nested fabrication method called "PRINT in PRINT" that emerged from the constraints of existing paste-extrusion 3D printers. Our nested printing strategy introduced a technique for robotic additive manufacturing of compound nonstandard architectural forms that are taller than the robot’s reachable area. These compound geometries consist of several smaller parts that nest within each other. By using the proposed method, the global geometry of a tower-like structure is divided into stackable components. When congruent surfaces are attained between the stacked pieces, the lower component shapes the upper one to preserve the adjacent bodies' tangential continuity. In other words, the inner side of a lower component in a stack is coincident with the outer side of the upper one. The design criteria are explained in more detail in the following design section.

Previous research projects used thin plastic shells as formwork to cast concrete (Burger et al. 2009; Naboni and Breseghello 2018). While the printed plastic dries fast and is expected to make it easy to cast concrete right after the print process, it is still wasteful and difficult to remove the plastic shell. Using a more sustainable material like clay as temporary formwork has some advantages over plastic. In particular, clay dissolves in water and can be easily removed and recycled.

Clay is a fragile material with mechanical properties that make it challenging to use it as a final product in the additive manufacturing of architectural forms. However, it does possess some interesting features that could be beneficial for temporary elements in additive manufacturing processes.

Fresh concrete placed adjacent to clay absorbs the clay's moisture over time, and consequently, the clay parts dry faster than air-drying. The fast-drying process results in a cracked and shattered surface on the clay that can be easily removed by hand, pressure-washed, or dissolved in water (Fig.4 c). This is similar to water-soluble materials used for temporary supports in 3D printing with plastic-based materials (Doyle and Hunt 2019). The PRINT in PRINT strategy uses clay as a temporary material to 3D print formworks for concrete elements.

Our method consists of three approaches, including Design Strategies, Fabrication Processes, and Assembly of a nested column as follows:

4.3.1. Design Strategies

By using our method, two types of geometries can be easily nested as a 3D composition, including closed and open forms. Here, a closed form refers to a geometry with an enclosed area and continues mass when an empty space is left in between. Such a geometry has a closed curve or polyline in its horizontal section. An open form is a geometry with a non-closed area with no defined space between its mass. Every closed form can be divided into several open forms. The focus of this paper is on closed forms; open forms are the subject of authors' future work. In this paper, we study a conical column with a twisted enclosure. This lofted geometry has an empty core.

The general design step is to intersect a geometry with a series of planes. In this paper, we use surfaces that are parallel to the initial construction plane. The number of the planes (n) and the distance between them (H) determine the number of nested components and the height of each component respectively (Figure 4.1 a). PRINT in PRINT strategy requires a few design criteria and can create any geometry that follows all below criteria:

- Each slice of the compound geometry should be slightly smaller than the one underneath, so they can nest within each other. In other words, the horizontal section of nested components at any height in the stack should not intersect the adjacent one (Figure 4.1 b).
- The global geometry can include zero, negative, positive, and double curvatures. If the curvature changes in the Z, the geometry should be sliced and fabricated in

separate stacks. In other words, all nested components in a stack must have consistent surface curvatures. The reason for this is that nested components should be taken out of their stack to be assembled later. A component with both positive and negative curvatures along its height can be created in this method but cannot be taken out of the stack (Figure 4.1 c). In their stack, nested components should be designed in a way that we can easily slide them out. Besides sliding the component linearly, it is possible to take out the nested pieces while rotating and moving them simultaneously.

- An important aspect of the proposed method is to design every component to be matched with its adjacent pieces, creating the desired form once assembled. Therefore, a given free-form geometry should be sliced when the top face of a lower component (S1) has the same shape as the upper module's bottom face (S2) (Figure 4.2). In this case, the seamless assembly of the final product is guaranteed.

The workflow in this paper includes a parametric algorithm for designing and slicing the geometry in Rhino and Grasshopper. HAL, a plugin for Grasshopper, was used to program the robot and create the toolpath.

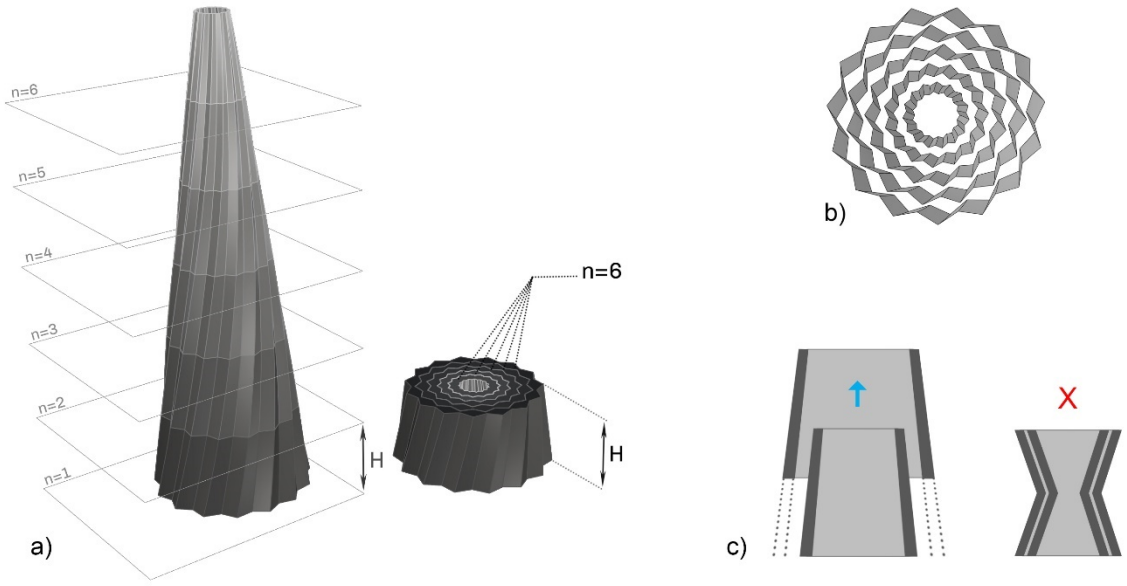

Figure 4.1: a) A series of horizontal planes slice the main geometry and break it into several components (n). The fixed distance between planes (H) defines the height of the nested mass. b) Com-ponents in a stack should not intersect. c) The curvature of the surface in each stack should be consistent, otherwise, the components cannot be taken out of the stack

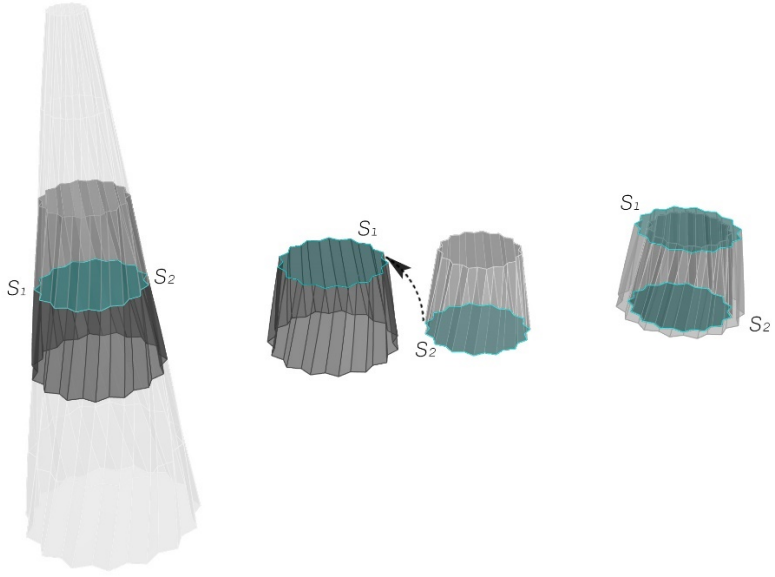

Figure 4.2: The lower component's top face (S1) and the upper component's bottom face (S2) are identical

4.3.2. Fabrication Processes

The nested components were created in two steps. A fast-setting concrete was cast between a series of shells that were robotically 3D printed with clay. The logic be-hind the design and fabrication of the nested components is that each piece of the compound geometry includes a thin outer shell, which, when nested within other pieces, creates the inner shell of the next component, and those shells together de-fine the boundaries of concrete cores (Figure 4.3). The outer shells were later dissolved in water so the concrete cores could be extracted for the assembly step. The concrete's thickness depends on both the design of the main geometry and the number of nested components (n). As the number of nested components increases, the resulting concrete cores are thinner, and the nested elements are shorter (H is smaller). The prototype presented in this paper had six components (n) with a height of 23 cm (H) in the nested stack. The thickness of the concrete in most of the components was 3 cm and the smallest one in the center of the mass was fabricated with a 1.5 cm thickness of the concrete to host the 5 cm steel structure.

The authors observed failure in building geometries with long straight segments in their horizontal section (Figure 4.4 a, b). Fabricating thin shells with long and tall straight segments resulted in either collapse or deformation of the printed object. One solution is to substitute straight segments with smaller zig-zag or chevron pat-terns in the design. Similarly, Burger et. al (Burger et al. 2020) reported a delamination issue with 3D printing a shell with plastic filaments. While clay remains soft for a while, pouring

concrete right away will destroy the soft shells. One solution is pouring concrete in multiple steps with limited height during or after the print process.

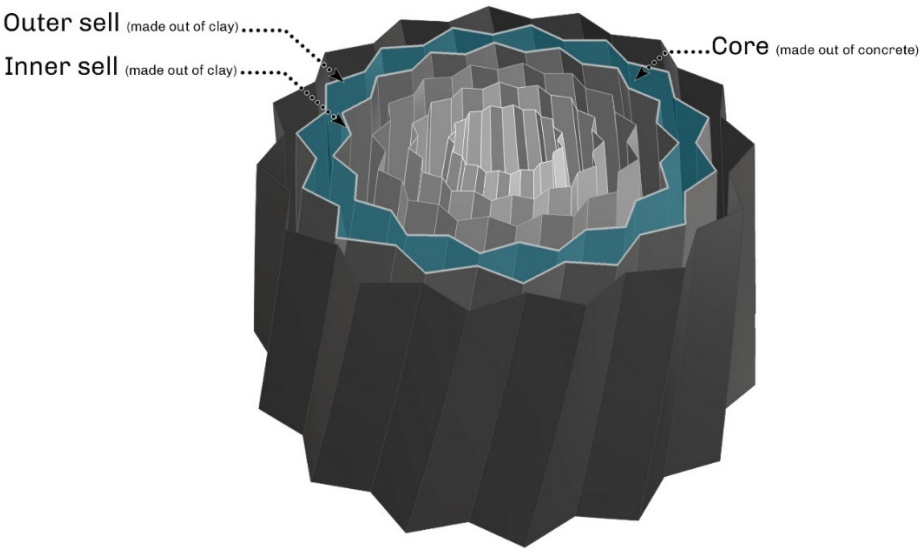

Figure 4.3: The clay shells create a temporary formwork for the concrete cores

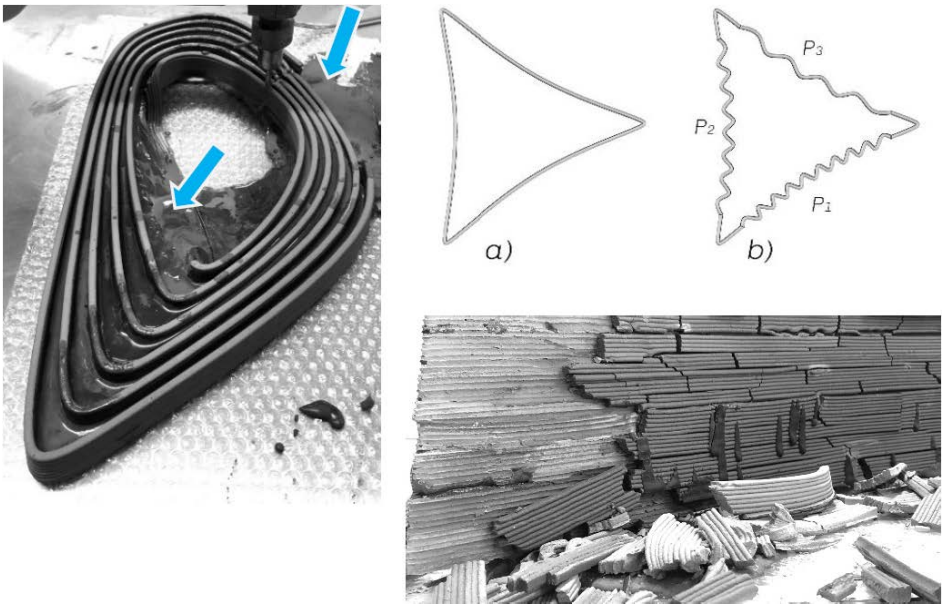

Figure 4.4: a, b) Zig-zag patterns are applied to increase the stability of the thin clay shells. c)The dried clay can be easily detached

IRB 1200 industrial robot, one of the smallest ABB robots, was used in this paper to 3D print a twisted column as proof of concept. The maximum height of the robot while holding an extruder perpendicular to the print bed is 70 cm. The column was built with 40 cm in diameter and 140 cm in height (Figure 4.5 a).

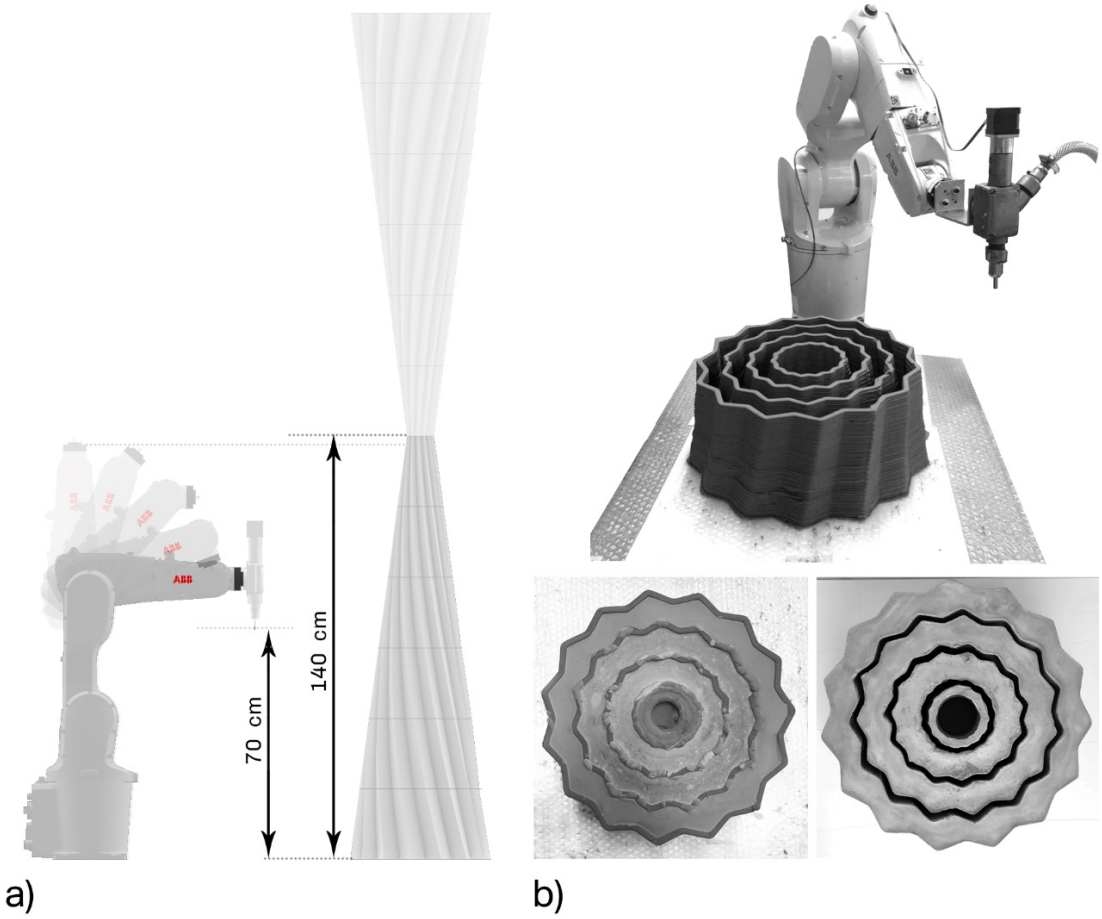

Figure 4.5: a) Height comparison between the robotic arm and the designed column. b) 3D Printing temporary shells, casting concrete, and removing the clay shells

In this experiment, after 48 hours, the concrete cores completely absorbed the clay shells' moisture in the lab environment, which had decent ventilation. Most of the

outer clay surface was removed manually while nested components were left in a bucket of water for 24 hours to dissolve the clay shells. While only 70% of the clay dissolved in water, the result was promising, and the concrete parts were extracted with gentle force and ultimately pressure-washed to remove the remaining clay (Figure 4.5 b).

4.3.3. Assembly

Since each concrete piece's bottom surface (S2) was identical to the top surface of the module underneath (S1), the assembly process was straightforward. The nested components were sequentially lifted, giving shape to the main geometry. Three scenarios can be imagined designing the connection between stacked components: First, the printed components can be connected to a network of cables to create a post-tension structural system. Second, concrete is cast in the hollow core of the com-pound geometry and reinforced with steel bars to shape a single homogenous com-ponent (Anton et al. 2019)**.** Finally, a separate steel structure can be employed to bear the structural loads and hold the compound geometry pieces together. The third approach was used in this paper, wherein an independent steel structure was de-signed, and the concrete components were fixed in place using bolts and steel spacers.

The flat surface under the nested components during the printing and casting process resulted in a clean flat surface at the bottom of concrete pieces. There were some minor imperfections on the top surfaces of the concrete components that re-quired a thin (2mm) gap between each piece to make it visually pleasing during the assembly process.

Steel spacers with a 10 mm offset from the edge of the concrete were used to create the gap and fix the parts in place (Figure 4.6).

Figure 4.6: The quality of the concrete elements and the detail of the independent steel structure

The assembly process was relatively easy and could be accomplished by a single individual on the Texas A&M University campus. (Figure 4.7).

Figure 4.7: Two twisted columns with a total height of 280 cm were robotically fabricated

4.4. Discussion

In this project, the goal was to establish a feedback loop between geometry, mate-rial, simulation, and fabrication. The design criteria explained in section 2.1 are the results of technical considerations in the proposed nesting method. Those rules push toward designing a tapered geometry with either negative or positive curvature or both, so the sliced components can easily nest within each other and be taken out of their stack later.

We were aware of the challenge of matching the concrete cast pieces together in the column when each of them came out of the nested mass and addressed the aesthetic concerns by adding steel spacers in the assembly process.

While HAL plugin was used to generate the robot toolpath, the degree of conformity to the desired geometry was afforded through the proposed algorithmic method, which translates the impacts of manipulation of successive layer width, thicknesses, and buildup rates into the robot's operation. Besides the size of our robot and the printing frame, the final printed geometry was influenced by various deposition parameters**.** Factors included controlling the rheology of the clay paste (Mansoori and Palmer 2018), deformation of a wet material deposited under a load generated by the subsequent layer deposition (Bard et al. 2012), surface contact between consecutive printing layers (Farahbakhsh et al. 2020), and restricted corbeling slope of overhanging sections to control structure buckling, as well as the drying time of the concrete mix (Buswell et al. 2018). While accomplishing the ease of transportation and cost reduction,

the entire twisted column and its stackable components were affected by the robot's size in the XY plane. Mounting the robot on an external axis will push the boundaries even further. The form, final look, and architectural expression of the column emerged from clay and concrete material properties.

Nesting components have three benefits: first, they minimize material consumption and waste, as each piece shares at least one surface with others. Second, this technique can be more affordable, as a robot can create complex geometries that are taller than the maximum reach of the robot in the Z direction. Third, the nested printing approach minimizes the length of the toolpath, where the robot does not extrude any material. In traditional fabrication approaches where the toolpath is not continuous, moving from one path to another adds to the total fabrication time. Nesting components minimize the travel time between separate paths.

Nesting a tall structure in shorter stacks decreases the volumetric dimensions[10] and consequently facilitates transportation in terms of the required space. In the prototype presented in this paper, the assembled column had a bounding box of 280x40x40 cm. Nesting the column in four stacks required a bounding box of 92x40x40 cm. This means the components can be carried out to the installation site with an SUV

[10] In the original paper (previously published at the *CAAD Futures 2021* Conference), it was concluded that the surface area decreases as the result of nesting components. Later after the discussion with the dissertation committee members, “surface area” was replaced with “volumetric dimensions” in this dissertation.

with a small cargo space rather than using a truck with a minimum 280 cm bed in length or height. (Figure 4.8).

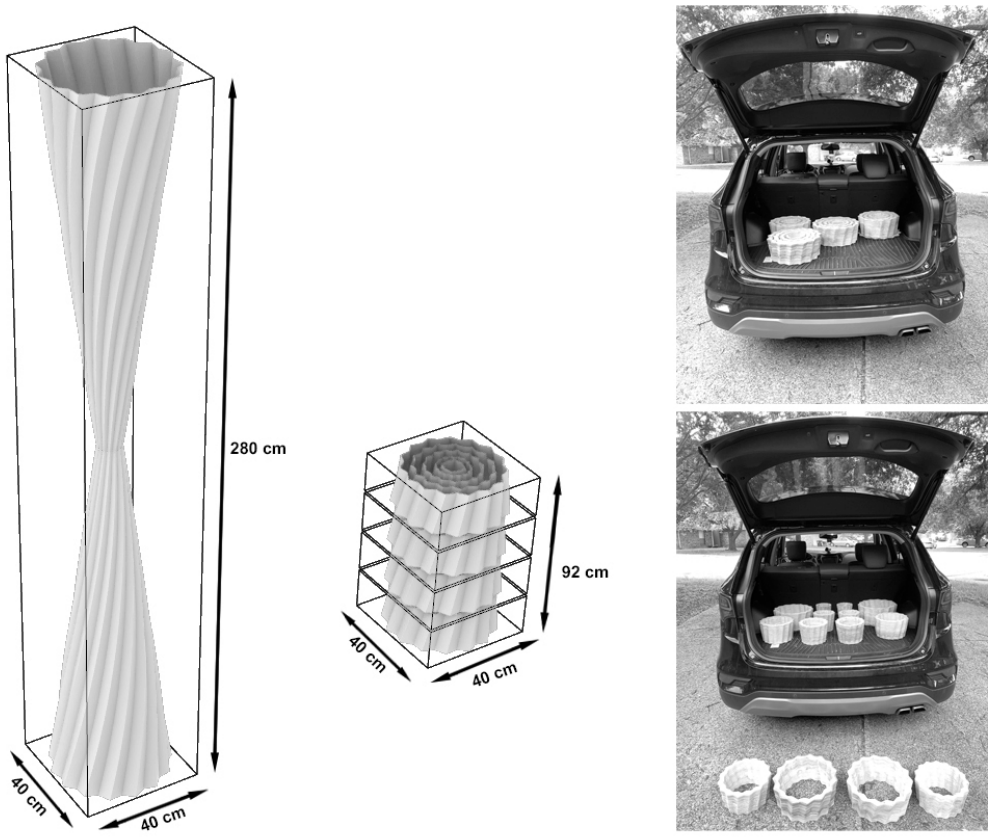

Figure 4.8: The nesting strategy decreases the volumetric dimensions and consequently requires less space for transportation

As long as the design criteria explained in this paper are followed, a designer can adopt a wide variety of geometries to make stackable tower-like structures in a nested fashion (Figure 4.9).

This paper aims to establish a link between the geometry of stackable components and clay 3D printing of a series of centric shells. While serving as the column surface constituents, these shells can be used as formworks of concrete bodies.

In this research, the printed clay serves as the formwork for concrete casting with promising results. While clay's moisture adjacent to cast concrete benefits the concrete's curing process, the dried clay shell can be easily removed. The authors will examine the possibility of using clay as a dissolvable support material for real-scale concrete printing, with plans to expand this work to a larger scope. Also, the authors aim to promote the following aspects in the future:

- Use the method to 3D print different building components on a larger scale,
- Investigate the best technique to reinforce components in the final assembly,
- Address the best way to joint adjacent components while providing the opportunity to disassemble the structure.
- Study the most convenient approach to assemble the component when using fewer tools, scaffolds or lifting mechanisms.
- Simulate the structural behavior of printed components and analyzing their performance.

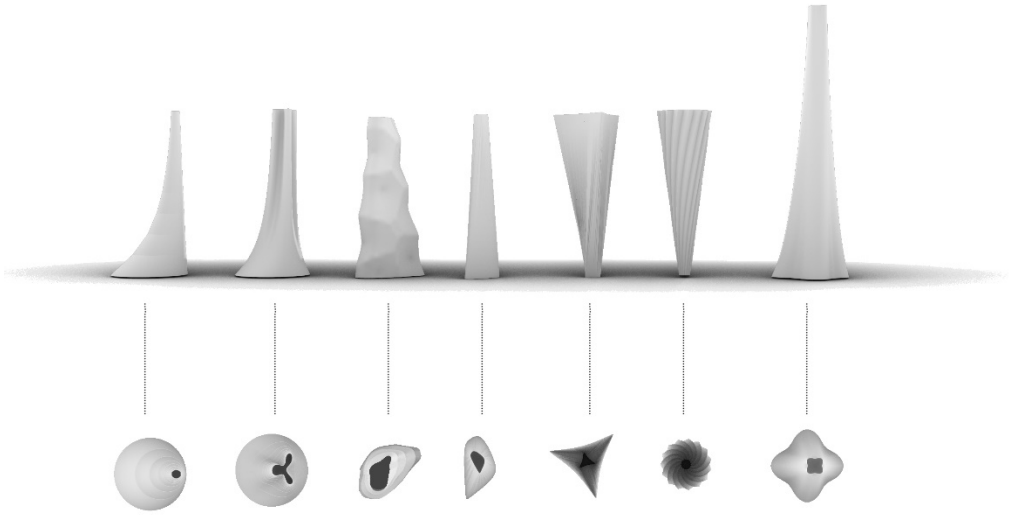

Figure 4.9: Various design options are explored and depicted in this picture

4.5. Conclusion

In addition to introducing the potential of nested 3D printing, the authors discuss the opportunities and challenges of using a small robot to fabricate an artifact larger than itself. By examining the merits of clay as a medium, hardware, and software details of the robotic system involved, this paper introduces the process of discretization of a twisted column into a limited number of uniquely shaped stackable components, showcasing a close tie between the column overall geometry, its final form, the number of its components, and the method of its fabrication.

The proposed method allows for constructing diverse 3D printed structures with complex surfaces, including zero, negative, positive, and double curvatures. The method can be applied to different types of components such as structural elements, cladding, complex shell structures, and interior surfaces.

On a broader scale, our proposed method can significantly reduce material waste, fabrication time, and production area while using a smaller printer to create artifacts larger than itself. Subsequently, lower investment in tools, facilities and resources will required. Since the method can generate the most compact components, the fabricated pieces occupy minimal storage space, and the pieces can be transported to the site in stacks. This process reduces both transportation and construction costs.

4.6. References

Anton, A., Yoo, A., Bedarf, P., Reiter, L., Wangler, T., Dillenburger, B.: Vertical Modulations Computational design for concrete 3D printed columns. Ubiquity Auton. - Pap. Proc. 39th Annu. Conf. Assoc. Comput. Aided Des. Archit. ACADIA 2019. 596–605 (2019).

Bard, J., Mankouche, S., Schulte, M.: Morphfaux: Probing the proto-synthetic nature of plaster through robotic tooling. ACADIA 2012 - Synth. Digit. Ecol. Proc. 32nd Annu. Conf. Assoc. Comput. Aided Des. Archit. 2012-Octob, 177–186 (2012).

Burger, J., Lloret-Fritschi, E., Scotto, F., Demoulin, T., Gebhard, L.: Research Collection. 3D Print. Addit. Manuf. 7, (2009). https://doi.org/10.1089/3dp.2019.0197.

Burger, J., Lloret-Fritschi, E., Scotto, F., Demoulin, T., Gebhard, L., Mata-Falcón, J., Gramazio, F., Kohler, M., Flatt, R.J.: Eggshell: Ultra-thin three-dimensional printed formwork for concrete structures. 3D Print. Addit. Manuf. 7, 49–59 (2020). https://doi.org/10.1089/3dp.2019.0197.

Buswell, R.A., Silva, W.R.L. De, Jones, S.Z., Dirrenberger, J., Leal de Silva, W.R., Jones, S.Z., Dirrenberger, J.: 3D printing using concrete extrusion: A roadmap for research. Cem. Concr. Res. 112, 37–49 (2018). https://doi.org/10.1016/j.cemconres.2018.05.006.

Craveiro, F., Duarte, J.P., Bartolo, H., Bartolo, P.J.: Additive manufacturing as an enabling technology for digital construction: A perspective on Construction 4.0. Autom. Constr. 103, 251–267 (2019). https://doi.org/10.1016/j.autcon.2019.03.011.

Doyle, S.E., Hunt, E.L.: Dissolvable 3D Printed Formwork. In: ACADIA. pp. 178–187 (2019).

Farahbakhsh, M., Kalantar, N., Rybkowski, Z.: Impact of robotic 3D printing process parameters on bond strength. 40th Annu. Conf. Assoc. Comput. Aided Des. Archit. ACADIA 2020. (2020).

ICON, https://www.iconbuild.com/vulcan, last accessed 2021/02/06.

Izard, J., Dubor, A., Hervé, P., Cabay, E.: Large Scale 3D Printing with Cable-Driven Parallel Robots. Constr. Robot. (2017). https://doi.org/10.1007/s41693-017-0008-0.

Keating, S.J., Leland, J.C., Cai, L., Oxman, N.: Toward site-specific and self-sufficient robotic fabrication on architectural scales. Sci. Robot. 2, (2017). https://doi.org/10.1126/scirobotics.aam8986.

Khoshnevis, B.: Automated construction by contour crafting, related robotics and information technologies. Autom. Constr. 13, 5–19 (2004). https://doi.org/10.1016/j.autcon.2003.08.012.

Mansoori, M., Palmer, W.: Handmade by Machine : A Study on Layered Paste Deposition Methods in 3D Printing Geometric Sculptures. (2018).

Naboni, R., Breseghello, L.: Fused Deposition Modelling Formworks for Complex Concrete Constructions. SIGraDi 2018. 700–707 (2018). https://doi.org/10.5151/sigradi2018-1648.

Nee, A.Y.C., Seow, K.W., Long, S.L.: Designing Algorithm for Nesting Irregular Shapes With and Without Boundary Constraints. Ann. ClRP. 107–110 (1986).

Rael, R., San Fratello, V.: Casa Covida, https://www.rael-sanfratello.com/made/casa-covida, last accessed 2021/02/06.

Zhang, X., Li, M., Lim, J.H., Weng, Y., Tay, Y.W.D., Pham, H., Pham, Q.C.: Large-scale 3D printing by a team of mobile robots. Autom. Constr. 95, 98–106 (2018). https://doi.org/10.1016/j.autcon.2018.08.004.

5. CONCLUSION

In addition to highlighting the importance of replacing concrete with a more sustainable material for large-scale additive manufacturing, this research investigates the opportunities and challenges of robotically assisted additive manufacturing of shell structures on both the macro- and meso-scales.

The first paper presented in Chapter two, set out to better understand the required steps to involve technical considerations in the design phase and to assess their impact on the structural integrity of 3D printed components. A four-step workflow (design, fabrication, digital reconstruction, and digital and physical analysis) was implemented to investigate the impacts of three process parameters on the interlayer bond strength in robotically assisted AM using a clay-based material. Three discrete scales—micro, mezzo, and macro—were introduced for investigating paste AM. Process parameters impact the bonding between successive layers at the meso-scale. These parameters can be involved in the architectural design and robot programming phase. In robotically assisted AM with paste, real-world material deposition is susceptible to environmental factors, which add a secondary geometric feature to the printed elements that was not included in the original digital model. A digital analysis method was introduced in the first paper to allow a deeper insight into impact of three selected process parameters on the interlayer bond strength. To further verify the validity of the digital analysis method, a destructive method based on the ASTM standard flexural tests for concrete and mortar

was used in conjunction with the digital analysis approach to compare and validate the results.

The second paper in Chapter three expanded on the destructive tests discussed in Chapter two. The difficulties associated with simulating and predicting AM processes in a digital analysis operation were described, and a series of destructive physical tests were employed to evaluate the 3D printed specimens and analyze the test results. Three selected process parameters (L, the distance between hypothetical nodes on the toolpath, H_2, the standoff distance of the nozzle, T, the delay time at each point) were systematically varied in the defined intervals and ninety-five components were 3D printed with a clay-based material. Manipulation of the process parameters was predicted to change the geometry of the layers at the meso-scale, simulate densification, and increase friction between successive layers in robotically assisted AM using paste.

Flexural test results revealed an average improvement of 41.2% when the H_2 parameter was varied within the specified range. The experiment did not detect any discernible effect of the T parameter on interlayer bond strength.

The first two papers that were presented in Chapters two and three focused on one of the most challenging issues at meso-scale related to the structural integrity of 3D printed objects using paste. The third paper detailed a problem at macro-scale in robotically assisted AM and delved into specifics of a nested robotic fabrication method that offers a design strategy to address the second research question in this dissertation. A case study was conducted to investigate the potential and challenges associated with

creating stackable geometries taller than the robot used. To the best of the author's knowledge, this was the first time a dissolvable formwork was made out of clay in a robotic additive manufacturing project. This study emphasized the significance of incorporating technical considerations of cutting-edge technology into the design phase, leading to design innovations and structural integrity.

5.1. Significance of the findings

The findings of the flexural tests and the analysis in Chapter Three revealed that periodically varying the H_2 parameter impacts the surface of the substrate at meso-scale and adds an interlocking-like feature between successive layers, increasing interlayer friction under shear. Several studies in the literature seek to improve the interlayer bond strength at the micro-scale. The results of the current study provide insights into the effectiveness and significance of geometrical approaches at meso-scale that have the capacity to serve even greater purposes when used in conjunction with micro-scale strategies.

5.2. Limitations of the research

The initial objective of this study was to use digital analysis techniques to evaluate the impacts of process parameters on the interlayer bond strength in AM with a clay-based material. The available finite element software, however, is currently limited. As the technology continues to improve, it will become much more feasible to simulate and predict the additive manufacturing processes and the performance of the printed material using physics-driven models. Furthermore, because the bonding between

successive layers of cement-based materials is affected by more intense chemical reactions than those between layers of the clay-based material used in this dissertation, additional research is required to expand and apply the findings of the current study to cement-based materials or similar materials that undergo chemical reactions while setting.

5.3. Future work

A foundation for research on large-scale robotically assisted additive manufacturing at the macro-scale has been presented.

That said, because Portland cement is currently the extrusive material of choice for large-scale 3D printing, it is important to also look into the effects of process parameters on interlayer bond strength for materials that experience chemical reactions during setting, such as cement.

Additionally, while this research included a case study for creating a stackable closed geometry using nested printing, future work should explore criteria that can provide opportunities for a greater variety of geometries.

APPENDIX

FLEXURAL STRENGTH TEST RESULTS

The following tables display the results obtained from the flexural tests of the 3D printed specimens and the mean (average) flexural strength for each series of specimens. As previously discussed in Chapter three, ninety-five specimens were 3D printed with a clay-based material. Specimens were first air-dried in the lab environment and then fired in the kiln at 1800 degrees of Fahrenheit for eight hours. In Group A, the impact of the H_2 parameter was studied, and in Group B, the impact of the T parameter was investigated.

Table 5.1: A0 series flexural test results

A0 Series		**D_n**	**T**	**B**	**D**	**Maximum Force**	**Strength**	**Mean**				
								D_n	**T**	**H2**	**Specimens**	**Mean Strength**
Test#	Specimen	(mm)	(mm)	(mm)	(mm)	(KN)	(MPa)	(mm)	(s)	(mm)		(MPa)
1	1a	8	0	54	53	1.32	**2.39**	8	0	0	A0-1	2.37
2	1b	8	0	58	56	1.64	**2.48**					
3	1c	8	0	53	53	1.21	**2.24**					
4	2a	16	0	60	58	1.72	**2.34**	16	0	0	A0-2	2.31
5	2b	16	0	59	56	1.53	**2.27**					
6	3a	24	0	55	52	1.4	**2.59**	24	0	0	A0-3	2.34
7	3b	24	0	61	59	1.62	**2.10**					
8	4a	32	0	72	54	1.66	**2.17**	32	0	0	A0-4	2.31
9	4b	32	0	70	52	1.69	**2.46**					
10	5a	40	0	56	58	1.33	**1.94**	40	0	0	A0-5	2.37
11	5b	40	0	51	55	1.57	**2.80**					

Table 5.2: A1 series flexural test results

A1 Series		D_n	H_2	b	d	Maximum Force	Strength	Mean			
								H_2	D_n	Specimen	Mean Strength
Test #	Specimen	(mm)	(mm)	(mm)	(mm)	(KN)	(MPa)	(mm)	(mm)		(MPa)
1	1a	8	6	56	55	1.95	**3.17**				
2	1b	8	6	61	61	2.98	**3.61**	6	8	**A1-1**	**3.39**
3	1c	8	6	55	56	2.13	**3.40**				
4	2a	16	6	55	57	2.46	**3.79**				
5	2b	16	6	55	56	1.86	**2.97**	6	16	**A1-2**	**3.09**
6	2c	16	6	61	61	2.09	**2.53**				
7	3a	24	6	57	55	1.9	**3.03**				
8	3b	24	6	61	59	3	**3.89**	6	24	**A1-3**	**3.46**
9	3c	24	6	55	56	2.17	**3.46**				
10	4a	32	6	56	77	3.8	**3.15**				
11	4b	32	6	54	72	3.32	**3.26**	6	32	**A1-4**	**3.20**
12	4c	32	6	55	73	3.41	**3.20**				
13	5a	40	6	50	55	1.77	**3.22**				
14	5b	40	6	51	55	1.85	**3.30**	6	40	**A1-5**	**3.26**
15	5c	40	6	50	56	1.86	**3.26**				

Table 5.3: A2 series flexural test results

A2 Series		D_n	H_2	b	d	Maximum Force	Strength	Mean			
								H_2	D_n	Specimen	Mean Strength
Test #	Specimen	(mm)	(mm)	(mm)	(mm)	(KN)	(MPa)	(mm)	(mm)		(MPa)
1	1a	8	14	68	69	4.18	**3.55**				
2	1b	8	14	68	67	4.43	**3.99**	14	8	A2-1	**3.73**
3	1c	8	14	69	68	4.22	**3.64**				
4	2a	16	14	67	65	2.83	**2.75**				
5	2b	16	14	67	67	3.6	**3.29**	14	16	A2-2	**3.02**
6	2c	16	14	67	64	3.01	**3.02**				
7	3a	24	14	61	68	2.76	**2.69**				
8	3b	24	14	66	61	3.68	**4.12**	14	24	A2-3	**3.41**
9	3c	24	14	64	66	3.46	**3.41**				
10	4a	32	14	78	62	3.11	**2.85**				
11	4b	32	14	79	61	3.58	**3.35**	14	32	A2-4	**3.10**
12	4c	32	14	77	62	3.32	**3.08**				
13	5a	40	14	60	57	2.28	**3.22**				
14	5b	40	14	57	56	2.12	**3.26**	14	40	A2-5	**3.24**
15	5c	40	14	56	59	2.3	**3.24**				

Table 5.4: A3 series flexural test results

A3 Series		D_n	H_2	b	d	Maximum Force	Strength	Mean			
								H_2	D_n	Specimen	Mean Strength
Test #	Specimen	(mm)	(mm)	(mm)	(mm)	(KN)	(MPa)	(mm)	(mm)		(MPa)
1	1a	8	22	80	80	6.89	**3.70**				
2	1b	8	22	Failed	Failed	NA	**NA**	22	8	**A3-1**	**3.70**
3	1c	8	22	Failed	Failed	NA	**NA**				
4	2a	16	22	77	77	5.31	**3.20**				
5	2b	16	22	74	70	4.07	**3.09**	22	16	**A3-2**	**3.14**
6	2c	16	22	74	75	4.74	**3.13**				
7	3a	24	22	75	67	5.17	**4.22**				
8	3b	24	22	75	69	3.38	**2.60**	22	24	**A3-3**	**3.41**
9	3c	24	22	73	69	4.3	**3.40**				
10	4a	32	22	90	68	5.38	**3.56**				
11	4b	32	22	86	62	3.21	**2.67**	22	32	**A3-4**	**3.11**
12	4c	32	22	84	66	4.14	**3.11**				
13	5a	40	22	63	58	2.6	**3.37**				
14	5b	40	22	59	59	2.44	**3.27**	22	40	**A3-5**	**3.32**
15	5c	40	22	57	56	2.16	**3.32**				

Table 5.5: B1 series flexural test results

B1 Series		D_n	T	b	d	Maximum Force	Strength	Mean			
								T	D_n	Specimen	Mean Strength
Test #	Specimen	(mm)	(s)	(mm)	(mm)	(KN)	(MPa)	(s)	(mm)		(MPa)
1	1a	8	0.6	56	55	1.67	**2.71**				
2	1b	8	0.6	55	57	1.65	**2.54**	1	8	**B1-1**	**2.54**
3	1c	8	0.6	58	57	1.63	**2.38**				
4	2a	16	0.6	55	51	0.12	**Failed**				
5	2b	16	0.6	51	54	1.27	**2.35**	1	16	**B1-2**	**2.36**
6	2c	16	0.6	55	52	1.28	**2.37**				
7	3a	24	0.6	55	52	0.95	**1.76**				
8	3b	24	0.6	61	58	1.49	**2.00**	1	24	**B1-3**	**2.01**
9	3c	24	0.6	51	53	1.18	**2.27**				
10	4a	32	0.6	71	52	1.21	**1.73**				
11	4b	32	0.6	74	59	1.58	**1.69**	1	32	**B1-4**	**1.71**
12	4c	32	0.6	70	51	1.13	**1.71**				
13	5a	40	0.6	47	50	1.01	**2.36**				
14	5b	40	0.6	58	56	1.52	**2.30**	1	40	**B1-5**	**2.32**
15	5c	40	0.6	50	55	1.26	**2.29**				

Table 5.6: B2 series flexural test results

B2 Series		D_n	T	b	d	Maximum Force	Strength	Mean			
								T	D_n	Specimen	Mean Strength
Test #	Specimen	(mm)	(s)	(mm)	(mm)	(KN)	(MPa)	(s)	(mm)		(MPa)
1	1a	8	1	59	58	2.13	**2.95**				
2	1b	8	1	55	59	2.18	**3.13**	1	8	**B2-1**	**3.13**
3	1c	8	1	55	53	1.86	**3.31**				
4	2a	16	1	58	56	1.89	**2.86**				
5	2b	16	1	60	58	2.04	**2.78**	1	16	**B2-2**	**2.79**
6	2c	16	1	58	58	1.94	**2.73**				
7	3a	24	1	61	56	1.33	**1.91**				
8	3b	24	1	57	55	1.38	**2.20**	1	24	**B2-3**	**2.21**
9	3c	24	1	62	57	1.84	**2.51**				
10	4a	32	1	76	57	1.66	**1.85**				
11	4b	32	1	71	59	1.65	**1.84**	1	32	**B2-4**	**1.85**
12	4c	32	1	74	57	1.62	**1.85**				
13	5a	40	1	54	56	2.16	**3.51**				
14	5b	40	1	60	59	2.13	**2.80**	1	40	**B2-5**	**2.82**
15	5c	40	1	58	56	1.42	**2.15**				

Table 5.7: B3 series flexural test results

B3 Series		D_n	T	b	d	Maximum Force	Strength	Mean			
								T	D_n	Specimen	Mean Strength
Test #	Specimen	(mm)	(s)	(mm)	(mm)	(KN)	(MPa)	(s)	(mm)		(MPa)
1	1a	8	1.6	The parameter values for this specimen resulted in an excessive accumulation of material and failed to produce an acceptable printed object.				2	8	**B3-1**	**NA**
2	1b	8	1.6								
3	1c	8	1.6								
4	2a	16	1.6	63	62	2.27	**2.58**				
5	2b	16	1.6	59	57	2.02	**2.90**	2	16	**B3-2**	**2.91**
6	2c	16	1.6	62	58	2.46	**3.24**				
7	3a	24	1.6	65	63	2.27	**2.42**				
8	3b	24	1.6	61	59	1.98	**2.56**	2	24	**B3-3**	**2.57**
9	3c	24	1.6	66	62	2.52	**2.73**				
10	4a	32	1.6	83	66	3.21	**2.44**				
11	4b	32	1.6	84	66	3.13	**2.35**	2	32	**B3-4**	**2.36**
12	4c	32	1.6	78	69	3.09	**2.29**				
13	5a	40	1.6	64	65	2.88	**2.93**				
14	5b	40	1.6	60	59	2.13	**2.80**	2	40	**B3-5**	**2.83**
15	5c	40	1.6	61	59	2.12	**2.75**				